Geomorphology 453 (2024) 109127

Contents lists available at ScienceDirect

Geomorphology

journal homepage: www.journals.elsevier.com/geomorphology

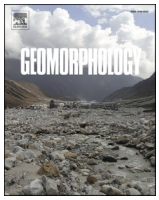

Variable downcanyon morphology controlling the recent activity of shelf-incised submarine canyons (Alboran Sea, western Mediterranean)

J. Cerrillo-Escoriza [a,b], F.J. Lobo [a,*], Á. Puga-Bernabéu [b], P. Bárcenas [c], I. Mendes [d], J.N. Pérez-Asensio [b], R. Durán [e], T.J. Andersen [f], Á. Carrión-Torrente [a,b], M. García [g], A. López-Quirós [b], M. Luján [h], A. Mena [i], O. Sánchez-Guillamón [c], M.J. Sánchez [j]

[a] Department of Marine Geosciences, Instituto Andaluz de Ciencias de la Tierra (CSIC-UGR), Avenida de las Palmeras, 4, 18100 Armilla, Granada, Spain
[b] Departamento de Estratigrafía y Paleontología, Facultad de Ciencias, Universidad de Granada, Campus de Fuentenueva s.n., 18002, Granada, Spain
[c] Instituto Español de Oceanografía, Centro Oceanográfico de Málaga (IEO-CSIC), Puerto Pesquero s/n Fuengirola, 29640 Málaga, Spain
[d] Centro de Investigação Marinha e Ambiental (CIMA), Rede de infraestrutura em Recursos Aquáticos (ARNET), Universidade do Algarve, 8005-139 Faro, Portugal
[e] Institute of Marine Sciences (CSIC), Passeig Marítim de la Barceloneta, 37-49, 08003 Barcelona, Spain
[f] Department of Geosciences and Natural Resource Management (IGN), University of Copenhagen, Øster Voldgade 10, DK-1350 Copenhagen K, Denmark
[g] Instituto Español de Oceanografía, Centro Oceanográfico de Cádiz (IEO-CSIC), Puerto Pesquero, Muelle de Levante, s/n, 11006 Cádiz, Spain
[h] Department of Earth Sciences, CASEM, Facultad de Ciencias del Mar y Ambientales, Campus Universitario de Puerto Real, Universidad de Cádiz, 11519 Puerto Real, Spain
[i] Departamento de Xeociencias Mariñas e Ordenacion do Territorio, Facultad de Ciencias do Mar Edif. CC Experimentais Campus Universitario, Universidad de Vigo, 36310 Vigo, Spain
[j] Instituto de Oceanografía y Cambio Global (IOCAG), Universidad de Las Palmas de Gran Canaria, Campus Universitario de Tafira Edif. Ciencias Básicas, 35017 Las Palmas de Gran Canaria, Spain

ARTICLE INFO

Keywords:
Submarine canyons
Sediment analysis
Underwater imagery
Seafloor mapping
Sediment transport
Alboran Sea

ABSTRACT

This research aims to distinguish genetic sedimentary processes building canyon geomorphological patterns and the factors driving different sedimentary activities in two nearby Mediterranean shelf-incised submarine canyons (Carchuna and Motril) that exhibit different degrees of incision on the narrow margin of the northern Alboran Sea.

The straight Carchuna Canyon incises the shelf up to 200 m off the coastline and exhibit steep canyon walls featuring narrow terraces, muddy sands with high contents of organic matter along the thalweg, and transported shelf benthic foraminifera in distal settings. The Motril Canyon head is wider and incises the shelf edge, ca. 2 km off the coastline. It exhibits a sinuous morphology and less steep walls, wider terraces, and higher sedimentation rates with muddy sediments along the thalweg. In both canyons, cross-section relief, width, incision, and area decrease downslope, although these parameters increase locally.

The downslope variations of geomorphological parameters are attributed to enhanced erosional/depositional processes promoted by tectonically controlled abrupt changes of the axial channel orientation. The degree of shelf incision, the location of the canyon heads in relation with the local sediment sources, and the seasonally variable hydrodynamic regimes determine the different degrees of recent canyon activity. The Motril Canyon is interpreted as a mature system that reflects episodic activity, collecting fine-grained sediments from the nearby Guadalfeo River. The Carchuna Canyon exhibits a youthful developmental stage whose activity is more continuous and involves sediment trapping of littoral cells and continuous downslope sand transport.

1. Introduction

Submarine canyons are common morphological features incised on continental margins (Daly, 1936; Shepard and Emery, 1941; Normark and Carlson, 2003; Harris and Whiteway, 2011) and constitute the main conduits for shelf-to-basin sediment transport (Shepard, 1981; Canals et al., 2004; Piper and Normark, 2009; Puig et al., 2014; Fisher et al., 2021). Sea-level changes play an important role in the evolution of

* Corresponding author.
E-mail address: francisco.lobo@csic.es (F.J. Lobo).

https://doi.org/10.1016/j.geomorph.2024.109127
Received 8 August 2023; Received in revised form 29 February 2024; Accepted 29 February 2024
Available online 5 March 2024

submarine canyons. Sequence stratigraphic schemes were initially based on the assumption that canyons were preferentially active during sea-level lowstands, when the continental shelves were subaerially exposed; the fluvial systems delivered directly into canyon heads, establishing a direct link between fluvial and deep-water systems (Mitchum Jr, 1985; Vail, 1987; Posamentier and Vail, 1988). Following this assumption, submarine canyons were regarded as essentially inactive during sea-level highstands. There is now strong evidence, however, that many submarine canyons were active during the Holocene highstand, when flows capable of transporting sediments modified canyon axial channels (e.g., Canals et al., 2006; Xu et al., 2008). Shelf width and steepness are major factors determining canyon activity during highstand periods. Canyon-head connectivity, being facilitated by steep and narrow shelves (Bernhardt and Schwanghart, 2021), controls the quantity and calibre of sediments transferred from coastal to deep-water environments, the nature of infill, and depositional processes at canyon heads (Gamberi et al., 2017).

The degree of canyon shelf incision essentially determines the amount of sediments deposited in shallow water that may be captured by the canyons (Mullenbach and Nittrouer, 2000; Puig et al., 2014, 2017; Sweet and Blum, 2016). Because shelf-incised canyons appear to be especially affected by erosive turbidity flows, they produce high rates of sediment export (Harris and Whiteway, 2011). Canyons that show evidence of recent activity tend to have their heads located a few kilometers (< 5–6) from the nearby shorelines, where canyon heads could be mantled by coarse-grained sediments (e.g., Lewis and Barnes, 1999; Mullenbach and Nittrouer, 2000; Normandeau et al., 2015; Sweet and Blum, 2016). In contrast, submarine canyons (whose heads are remote to the shoreline) are generally inactive and characterized by muddy sediments (Harris and Whiteway, 2011; Sweet and Blum, 2016). Shelf-incised canyon activity is also decisively influenced by the location of the canyon head with respect to the principal sedimentary source (Bernhardt and Schwanghart, 2021): longshore-drift-, river- or delta-fed (Sweet and Blum, 2016). The highest activity is usually related to a direct connection to terrestrial drainage systems (Babonneau et al., 2002; Brothers et al., 2013), which results in the channeling of hyperpycnal flows (Puig et al., 2017). Such a connection is particularly frequent in active margins characterized by high river discharges (Harris and Whiteway, 2011; Bernhardt and Schwanghart, 2021). Alternatively, sediments transported by shelf processes can be captured, depending on the strength and location of littoral cells or the occurrence of muddy depocenters (Sweet and Blum, 2016).

The dominance of sedimentary processes in shelf-incised canyons is reflected in the submarine morphology. Broad transitions from proximal erosional zones to distal depositional zones are usually found (Arzola et al., 2008; Lastras et al., 2009). This along-canyon trend is also seen in thalweg longitudinal downslope profiles, mainly having very concave shapes owing to continuous supply of coarse-grained sediments, regardless of the sea-level stand (Covault et al., 2011). Other characteristic features of shelf-incised canyons include deeply entrenched channels flanked by terraces and/or gullies, and highly variable alternates of erosional and depositional features in lower reaches (Arzola et al., 2008; Gamberi et al., 2017). Ultimately, the balance between erosive flows and hemipelagic deposition in a given canyon domain will determine the functioning of the system as a sediment conduit or sediment trap during highstand conditions (Drexler et al., 2006; Arzola et al., 2008; DeGeest et al., 2008).

Mediterranean submarine canyons constitute a distinctive population in oceanic regions. They display the smallest mean lengths, depths of incision, average areas, and canyon spacing (Harris and Whiteway, 2011; Amblas et al., 2018). Their distinctiveness stems from the fact that the canyon genesis was dictated by a pronounced sea-level lowering and desiccation during the Messinian Salinity Crisis (Harris and Whiteway, 2011). Shelf-incised canyons are therefore remarkable in the Mediterranean active margins (Bernhardt and Schwanghart, 2021), where: (a) a regional correlation with regionally-averaged sediment discharges to the coast has been found (Harris and Macmillan-Lawler, 2015); and (b) their evolution is largely driven by erosive density currents (Bernhardt and Schwanghart, 2021).

The northern margin of the Alboran Sea (western Mediterranean Sea) exhibits an abrupt character, with a narrow shelf and the sculpting of several sectors by submarine canyons and other valley systems (Vázquez et al., 2015). In this study, we present a detailed report of the morphology and recent sedimentary processes in two nearby shelf-incised submarine canyons. The shelf-incised, sinuous Motril Canyon is located 2 km off the shoreline, whereas the straight Carchuna Canyon dissects the entire shelf. In spite of their proximity and sharing the same margin, the studied canyons exhibit great geomorphologic and sedimentary differences. How each canyon acts depends on several complex factors that vary laterally within just a few kilometers and can control the evolution of the submarine canyons over time.

We aim to highlight geomorphological and sedimentary differences between these two nearby canyons and elucidate their respective roles in recent patterns of sediment transport and accumulation. Consequently, the specific objectives of this study are: (1) to discern the relation between sedimentary processes and canyon morphology; (2) to establish the driving factors of recent activity in both submarine canyons.

2. Study area

2.1. Geological setting

The Alboran Basin is a narrow, elongated basin located in the westernmost part of the Mediterranean Sea (Fig. 1A and B). A conjugate system of strike–slip and normal faults developed in the wake of the compressive setting since the late Oligocene (Fig. 1C) (Comas et al., 1999; Ballesteros et al., 2008). Moreover, the basin has been progressively restricted due to uplift of the adjacent mountainous reliefs composing the Gibraltar Arc (Platt and Vissers, 1986; Comas et al., 1992; García-Dueñas et al., 1992; Estrada et al., 1997; Platt et al., 2003). The Messinian Salinity Crisis produced an important sea-level lowering and desiccation of the Mediterranean Sea in the late Miocene that exposed most of the basin margins favoring the fluvial subaerial erosion and creating incipient canyons that were further developed by submarine erosional processes (Ryan et al., 1973; Frey-Martinez et al., 2004; Maillard et al., 2006; Juan et al., 2016; Gómez de la Peña et al., 2021).

The study area is located in the central sector of the northern Alboran Sea margin, between the towns of Motril and Calahonda (Fig. 1B-D). This sector comprises the narrowest shelf (3 km wide) of the entire northern Alboran Sea margin, which is deeply incised by the Motril and Carchuna canyons (Fig. 1C and D). The geological basement of the study area is composed of Paleozoic schists, Permo-Triassic phyllites, and Triassic marbles (Aldaya et al., 1979; Aldaya, 1981).

2.2. Coastal to shallow-water depositional systems

Sediment supply to coastline along the northern margin of the Alboran Sea has mainly been provided via relatively short, mountainous rivers (Liquete et al., 2005) that feed different shelf deltaic systems. Laterally, deltaic deposits are substituted by beach ridges, spit bars, and infralittoral prograding wedges (IPWs) (Ercilla et al., 1994; Hernández-Molina et al., 1994).

In the study area, the coastal sedimentary record contains Upper Pleistocene to Middle Holocene alluvial fans composed of conglomerates, and sandy Holocene deposits such as spit bars and IPWs (Lario et al., 1999; Fernández-Salas et al., 2009; Bárcenas et al., 2011; Ortega-Sánchez et al., 2014). Specifically, the Carchuna IPW —composed of coarse-grained sediments— exhibits a break in the slope at 20 m water depth, and is laterally bounded by the Carchuna Canyon head (Fig. 1C) (Fernández-Salas et al., 2009; Ortega-Sánchez et al., 2014). A submarine prodeltaic system off the Guadalfeo River is located west of the Motril

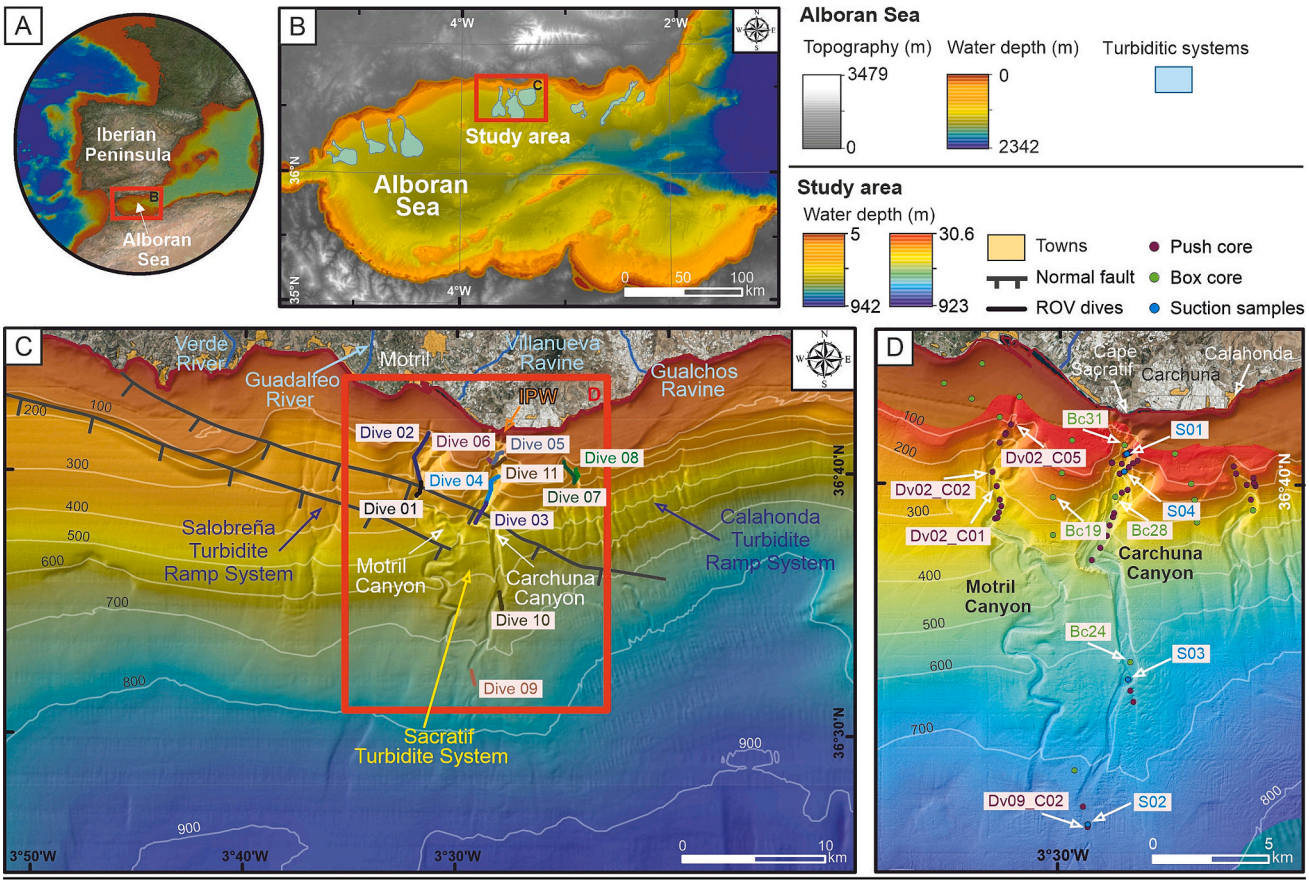

Fig. 1. (A) Geographic location of the Alboran Sea in the southern Iberian Peninsula. (B) Overview map of the Alboran Sea indicating the study area in the northern margin and the main turbiditic systems. (C) Location of the study area covered by the oceanographic survey ALSSOMAR 2019. A 50 m resolution bathymetric grid (Ministerio de Pesca, Agricultura y Alimentación, 2002) shows two turbiditic ramp systems (Salobreña and Calahonda), the Sacratif Turbidite System comprising the Motril and Carchuna canyons, and normal faults cutting the studied canyons (after Rodriguez et al., 2017). The site of Remote Operating Vehicle (ROV) dives is also marked. Aerial continental photography shows major rivers and towns. IPW: Infralittoral Prograding Wedge. (D) Location of push and box cores and suction samples over a 10 m resolution bathymetric grid acquired during the oceanographic survey ALSSOMAR 2019. The names of the sediment cores used for foraminifera identification and sedimentation rates are indicated. Bathymetric contours in meters.

Canyon head over the shelf (Jabaloy-Sánchez et al., 2014; Lobo et al., 2015).

2.3. Submarine valleys and deep-water depositional systems

The northern margin of the Alboran Sea contains several deep-water turbidite systems (Ercilla et al., 1992, 1994; Alonso and Ercilla, 2002a), contourite drifts, and mass-transport deposits (Ercilla et al., 2016, 2019). Turbidite systems formed by shelf-incised or shelf-edge canyons with channel-levee complexes and deep-water fans, and turbidite ramp systems with small-sized straight canyons and gullies eroding the slope that feed fan lobes are grouped into three different sectors (Fig. 1B): western, middle, and eastern (Vázquez et al., 2015).

The study area is located in the middle sector off the coast of Granada province and has several deep-water turbidite systems (Fig. 1C). The Sacratif Turbidite System includes the Motril and Carchuna canyons (Fig. 1C and D; Cerrillo-Escoriza et al., 2023). Motril Canyon is located 5 km east of the Guadalfeo River mouth, its main valley exhibiting a sinuous morphology on the slope. The rather straight Carchuna Canyon crosses the entire shelf and is located 200 m offshore Cape Sacratif. Both systems debouch into large lobes fed by distributary channels (Pérez-Belzuz and Alonso, 2000; Pérez-Belzuz et al., 2000) having superimposed sediment wave fields (Muñoz et al., 2017).

2.4. Oceanographic regime

The northern Alboran Sea is a microtidal, low energy wave setting (Parrilla and Kinder, 1987). Easterly winds are more common than westerly ones, although waves from the west-southwest are somewhat more energetic (Jabaloy-Sánchez et al., 2014). Littoral drift shows substantial variability due to the local coastal morphology and meteorological conditions (e.g., Stanley et al., 1975; Bárcenas, 2013).

The vertical water mass structure exhibits four main layers: Surface Atlantic Water (SAW), Western Intermediate Water (WIW), Levantine Intermediate Water (LIW), and Western Mediterranean Deep Water (WMDW) (Brankart and Pinardi, 2001; Millot, 2009, 2014). The SAW enters the Mediterranean Sea through the Strait of Gibraltar, where it is mixed with Mediterranean waters and generates the Atlantic Jet (AJ; velocities up to 1 $m \cdot s^{-1}$) triggering two anticyclonic gyres and one cyclonic gyre in the Alboran Sea (Tintoré et al., 1988; Perkins et al., 1990; García-Lafuente et al., 1998; Renault et al., 2012). In shallow water, the path of the AJ is controlled to a large extent by the wind regime (Sarhan et al., 2000; Oguz et al., 2017).

The coast along the study area is affected by wave trains coming from W, WSW, SW, ESE and E, oblique to the main E-W coastal trend (Ortega-Sánchez et al., 2014). The Carchuna Canyon head influences the coastal swell and storm-related processes as it increases nearshore wave heights, particularly of western waves, favoring long-term coastal erosion owing to energy concentration (Ortega-Sánchez et al., 2014). In addition, a bottom flow distinct to the wind-driven surface flow has been detected

in the Carchuna Canyon; in the bottom layer, the currents tend to flow downcanyon, particularly during easterlies dominance, where bottom flow velocities are between 20 and 30 cm·s^{-1} (Serrano et al., 2020).

2.5. Recent to modern sedimentary processes

Different sedimentary processes driven by postglacial climatic conditions took place in the Alboran Sea during the Quaternary. A first phase of turbiditic activity in submarine canyons was marked by an increase of fine-grained detritus due to either local ice melting or increased storminess during the Bølling-Allerød (Weaver and Pujol, 1988; Bozzano et al., 2009). A second phase of reactivation of submarine canyons was linked to glacial meltwater and riverine input during the Younger Dryas (Jimenez-Espejo et al., 2008; Bozzano et al., 2009).

At present, detrital material is delivered to the northern Alboran Sea margin by short rivers and ephemeral creeks, especially during autumn and winter (Stanley et al., 1975; Fabres et al., 2002; Palanques et al., 2005). Along submarine canyons, particle fluxes in nepheloid layers have been related to river floods (Palanques et al., 2005) or to the interaction of internal waves with the submarine morphology (Puig et al., 2004).

3. Materials and methods

Datasets used for this study were mostly collected during the ALSSOMAR-S2S multidisciplinary expedition carried out in August–September 2019 aboard the RV "Sarmiento de Gamboa".

3.1. Datasets

3.1.1. Bathymetric data

Multibeam bathymetric data were collected along the study area using a quill-mounted Atlas Hydrosweep DS™ multibeam echo sounder operating at frequencies of 14.5 to 16 kHz, providing coverage of up to six times the water depth. Raw multibeam data were processed with Teledyne Caris™ HIPS and SIPS Hydrographic Data Processing System and gridded to obtain Digital Elevation Models with cell sizes of 40, 30, and 10 m. These data were combined with background bathymetric data from the shelf (5 m resolution grid) as well as with an Alboran Sea bathymetric mosaic of 50 m resolution (Ministerio de Pesca, Agricultura y Alimentación, 2002) (Fig. 1C and D).

3.1.2. Seafloor imagery

High- and low-resolution photos and video footage were acquired in eleven dives by means of a standard definition video camera mounted on the Remote Operating Vehicle–ROV Luso (EMEPC—Portuguese Task Group for the Extension of the Continental Shelf). The ROV Luso was equipped with laser pointers with a laser beam spacing of 62 cm to provide references for scale, and an ultra-short baseline positioning system to ensure detailed records of the ROV tracks.

Video dives encompassed (Fig. 1C): (a) the upper segment of the Motril Canyon along two 5 km long continuous dives from the canyon thalweg (Dive 01) to the canyon head (Dive 02); in between, the dives run along the western canyon flank; (b) the upper (Dives 03, 04, 05, 06, and 11) and lower segments of the Carchuna Canyon (Dives 9 and 10), with 9 km in total length; and (c) the upper segment of a canyon of the Calahonda Turbidite System along 3 km long dives (Dives 7 and 8).

3.1.3. Sediment samples

Surficial sediment samples were collected with a suction arm and surficial rock samples were collected with a plier arm, both of them installed in the ROV (Fig. 1D). Up to 30 cm long sediment cores were collected with a push corer also mounted on the ROV, and handled by the plier arm (Fig. 1D). Up to 50 cm long sediment cores were collected by deploying a box corer from the ship (Fig. 1D). Sediment cores were initially split and the visual description of sedimentary facies was undertaken. The top first centimeters of these short sediment cores were subsequently sampled for grain-size analysis, determination of organic matter and carbonate contents, and foraminifera identification. Three sediment cores were sampled for the determination of sedimentation rates using ^{210}Pb and ^{137}Cs radioactivity measurements.

3.1.3.1. Grain size. Surficial sediment samples were dried in the oven at 60 °C to reach constant weight. Organic matter oxidation with hydrogen peroxide (H_2O_2 33 %) was carried out; later, approximately 10–15 g of sample were weighed. The samples were mixed with pyrophosphate 2 % in order to disintegrate and disperse fine sediments. Once the samples were disaggregated, 2 mm mesh size wet sieving was carried out with dispersant. The fraction >2 mm was dried in the oven at 60 °C until reaching constant weight, then weighed and labeled for storage. The fraction <2 mm was analyzed with a particle size analyzer by laser diffraction (MasterSizer 3000, Malvern®).

The grain size distribution was estimated according to the logarithmic Udden-Wentworth grade scale (Udden, 1914; Wentworth, 1922) and plotted as frequency versus grain size. These data were subjected to statistical analysis: mean, sorting, skewness, and kurtosis (Folk and Ward, 1957). Finally, grain size data were plotted according to the textural classification of sediments (Folk, 1954).

3.1.3.2. Geochemical analysis. Geochemical analysis entailed using the loss on ignition (LOI) method (Dean Jr, 1974; Bengtsson and Enell, 1986) to estimate organic matter and carbonate content of the surficial sediment samples. The LOI method is based on the sequential heating of the samples in a muffle furnace. After oven sediment drying to constant weight and determination of the water content (usually 12–24 h at 100 °C), organic matter was combusted to ash and carbon dioxide at 500–550 °C during 4 h.

In a second knickpoint, carbon dioxide was detached from carbonate (leaving oxide) by heating the samples to 900–1000 °C during 2 h. Assuming a weight of 44 g·mol^{-1} for carbon dioxide and 60 g·mol^{-1} for carbonate, the weight loss by LOI at 950 °C multiplied by 1.36 should equal the weight of the carbonate in the original sample.

3.1.3.3. Sedimentation rates. The analyses of sedimentation rates were performed along three short sediment cores located at the same latitude but in different physiographic locations: thalweg of the Motril Canyon, thalweg of the Carchuna Canyon, and intercanyon area between the studied canyons. The three sediment cores, Dv02_C02, BC19, and BC28 (respectively 18, 20, and 32 cm long) (Fig. 1D), were sampled each centimeter, and the samples were freeze-dried during 48–72 h to estimate the water content.

The samples were subsequently studied to assess the activity of ^{210}Pb, ^{226}Ra, and ^{137}Cs via gamma spectrometry at the Gamma Dating Center, Department of Geosciences and Natural Management, University of Copenhagen, Denmark. Measurements were carried out on a Canberra ultralow-background Ge-detector. ^{210}Pb was measured via its gamma-peak at 46.5 keV, ^{226}Ra via the granddaughter ^{214}Pb (peaks at 295 and 352 keV), and ^{137}Cs via its peak at 661 keV. Chronologies were calculated using the CRS-model by Appleby and Oldfield (1978). Activities in the lower part of the cores were calculated based on regressions of unsupported Pb-210 versus cumulated mass depth following the procedures described by Appleby (2001) and Andersen (2017).

3.1.3.4. Surficial foraminifera. The uppermost centimeter (0–1 cm) of 4 push cores and 3 box cores collected in the Motril (Dv02_C01, Dv02_C02, and Dv02_C05) and Carchuna canyons (Bc24, Bc28, Bc31, and Dv09_C02) (Fig. 1D) were used for benthic and planktonic foraminifera identification.

For surficial samples collected with the ROV suction arm, at least 300 benthic foraminifera were counted and identified at the species level in the fraction higher than 125 μm. Relative abundances (%) were

calculated from raw counts. Species with a relative abundance higher than 1.5 % were included in benthic foraminiferal assemblages. Four suction samples collected by the ROV were studied along the Carchuna Canyon (Fig. 1D). Two samples are from the upper part of the eastern wall (S01 and S04; Fig. 1D) and two samples pertain to the canyon thalweg of the lower segment (S02 and S03; Fig. 1D).

Transported shelf taxa include species whose deepest living depth (i.e., the deepest limit of its bathymetric range) was shallower than the sampling depth. These transported shelf taxa were grouped as total transported shelf taxa and identified along the Carchuna Canyon. Furthermore, the percentage of planktonic foraminifera (%P hereafter) was calculated using the following formula: [P / (P + B)] x 100, where P are planktonic foraminifera and B are benthic foraminifera.

3.2. Interpretation procedure

3.2.1. Bathymetric data

The bathymetric grids were imported into ArcGIS™ geographic information software and geo-spatial QPS Fledermaus™ software for geomorphological interpretations and detailed morphometric analysis in order to identify major sediment transport pathways and to determine the efficiency of sediment dispersal systems from the shelf to the slope through submarine canyons. The terminology defined by Paull et al. (2013) is used to describe the major geomorphological features of the studied submarine canyons. Geomorphological segments were defined in the Motril and Carchuna canyons according to the orientation of the axial channel and the slope gradient of the flanks.

3.2.2. Morphometrics

The main canyon morphometric parameters were measured in a number of bathymetric sections. We initially traced two parallel straight lines in intercanyon areas parallel to the path of the submarine canyons; afterwards, perpendicular lines 100 m apart were traced along both submarine canyons. Water depth and gradient values were measured each 10 m along the perpendicular lines. Bathymetric profiles along the thalweg of both studied canyons were classified according to Covault et al. (2011).

The main metric and morphologic characteristics of the canyons were measured so as to compare the type and canyon morphology in the study area (Table 1). The following parameters were measured: minimum and maximum water depth, total and straight canyon length, canyon sinuosity, canyon and canyon floor width, canyon incision, canyon area, canyon gradient, gradient of the canyon flanks, number of gullies that erode the canyon walls, and north azimuth. Canyon relief was quantified after Goff (2001) and Green et al. (2007). The average canyon relief was estimated by the RMS relief, which determines the square root of the profile variance between the canyon thalweg and adjacent interfluves.

3.2.3. Seafloor imaging

The images were placed geographically in an ArcGIS environment to aid in the characterization of submarine canyon seafloor features, in terms of grain size, overall lithology, and small-scale bedforms, and to aid in sedimentary facies analysis.

3.2.4. Sediment samples

Grain size and geochemical analysis served as ground truth of seafloor imagery and to provide genetic constraints and sediment sources of seafloor sediments and rocks. Foraminiferal assemblages were used to identify transported shelf taxa in deep areas of the submarine canyons. A comparison of sedimentation rates in different bathymetric settings (canyon versus intercanyon) was used to establish the recent activity of submarine canyons.

Table 1
Summary of the main metric characteristics of the submarine canyons in the study area.

C	Longitude (W)	Latitude (S)	L (m)	SL (m)	S	mD (m)	MD (m)	MW (m)	AvW (m)	FlW (m)	I (m)	CGr (°)	GrW (°)	GrE (°)	MGrW (°)	MGrE (°)	G	Az
Motril	3°31′15.51″	36°42′1.32″	26,944	20,945	1.28	66.49	763.84	4660	1560	1090	179	2.22	6.65	6.08	16.73	16.35	17	175.75
Carchuna	3°28′34.34″	36°41′41.02″	20,366	17,677	1.15	18.42	749.33	4020	1230	2160	226	2.39	9.67	8.06	33.88	24.55	49	182,38

C: canyons; L: total length (distance between the shallowest part of the canyon head and the deepest part of the canyon mouth measured along the canyon thalweg); SL: straight length (shortest distance between the shallowest part of the canyon head and the deepest part of the canyon mouth); S: sinuosity (relationship between the total and straight length); mD: minimum depth (depths at which canyon commences); MD: maximum depth (depth at which canyon ends); MW: maximum width (maximum horizontal distance perpendicular to the canyon valley between the highest part of the interfluves); AvW: average width (average value of canyon width measured along the canyon valley); FlW: maximum floor width (maximum distance across the canyon floor measured perpendicular to the canyon axis); I: maximum canyon incision (depth difference between the canyon axis and the adjacent interfluves); CGr: average canyon gradient (average angle measured between two points along the canyon axis relative to horizontal); GrN: average gradient of the northern canyon wall (average angle measured between the shallowest and deepest points along the northern canyon wall relative to horizontal); GrS: average gradient of the southern canyon wall (average angle measured between the shallowest and deepest points along the southern canyon wall relative to horizontal); MGrN: maximum gradient of the northern canyon wall; MGrS: maximum gradient of the southern canyon wall; G: number of gullies; Az: azimuth (orientation relative to north between the starting and ending points).

4. Results

4.1. Geomorphology

4.1.1. Major morphological features

The continental margin enclosed in the study area has a main E-W orientation and the shelf is up to 3.5 km wide (Figs. 1 and 2). The shelf edge is located at 100 to 125 m water depth. The Motril and Carchuna canyons are N-S trending, shelf-incised features that exhibit contrasting morphological configurations (Fig. 2).

4.1.1.1. Motril Canyon. The Motril Canyon is incised in the shelf edge, and its head lies at 100 m water depth, 2200 m off the northern coastline and 5500 m southeast of the Guadalfeo River mouth (Figs. 1C and 2A). Three geomorphological segments can be discerned in the Motril Canyon (Fig. 2; Table 2). The upper segment is characterized by a roughly N-S trending axial channel from 75 to 400 m water depths. The canyon head begins with a 950 m long and 140 m wide straight channel that incises the outer shelf up to 100 m water depth (Fig. 2B; Table 2). The amphitheater-like canyon head is excavated in the outer shelf and upper slope down to 275 m water depth that includes two large tributary channels on the eastern flank, and one tributary channel and wide terrace in the western flank (Table 2).

The middle segment starts with an abrupt change in the orientation of the main valley from N-S to NW-SE down to 500 m water depth. Here, the axial channel shows a sinuous path with two large terraces in the southwestern flank (Fig. 2B; Table 2). The lower segment trends N-S from 500 to 750 m water depths, and features six meanders. The width of the axial channel —limited by steep walls (ca. 16°)— decreases downslope from 900 to 300 m (Table 2). Away from the axial channel, lateral levees with superimposed bedforms are observed in the eastern flank (Fig. 2A). Downslope of the channel mouth (up to 900 m water depth), a lobate morphology is observed (Fig. 2A).

4.1.1.2. Carchuna Canyon. Two geomorphological segments were distinguished in the Carchuna Canyon (Fig. 2; Table 2). In the upper segment, the canyon is deeply incised in the shelf, as its head is located just 200 m off the coastline at 30 m water depth (Figs. 2B and 3). This segment is defined by an axial channel with a main N-S orientation down to 500 m water depth. The canyon head starts with an axial channel that widens from 70 to 150 m down to 200 m water depth and it widens to as much as 550 m. The uppermost axial channel exhibits bedforms that may reach 2 m in height and 15–30 m in length (Fig. 3). The eastern flank in the shelf-incised section harbors three tributary channels, whose heads are incised into shelf infralittoral prograding wedges (Fig. 3; Table 2).

Downslope, the eastern flank becomes steeper (ca. 35°), with short terraces (Fig. 2B; Table 2). The western flank in the uppermost shelf-incised section is even steeper (ca. 40°) and contains several gullies, plus two tributary channels (Fig. 3; Table 2). This flank becomes smoother downslope, having elongated and narrow terraces limited by steep walls (ca. 20°) (Fig. 2B; Table 2). The transition between the upper and lower segments is marked by an abrupt change of orientation of the main valley from NNE-SSW to WNW-ESE (Fig. 2). The lower segment is characterized by a straight and wide valley with a main N-S orientation until 740 m water depth. The axial channel is limited by two large lateral levees (Table 2). At 620 m water depth, the orientation of the axial channel shifts to the NNE-SSW. Superimposed undulations are identified over the eastern levee (Fig. 2A; Table 2). The axial channel exhibits a sinuous path between 645 and 730 m water depth (Table 2). Downward from the channel mouth, a lobe, merged with the equivalent feature of the Motril Canyon, extends to 900 m water depth (Fig. 2A).

4.1.2. Morphometric parameters

The longitudinal profile of the intercanyon area is slightly convex; its slope gradient ranges from 11° close to the shelf edge to 2° downslope. The main knickpoints are located on the shelf edge and at 14 km from the coastline in the lower reaches of the intercanyon (Fig. 4).

4.1.2.1. Motril Canyon. The Motril Canyon is almost 27 km long and

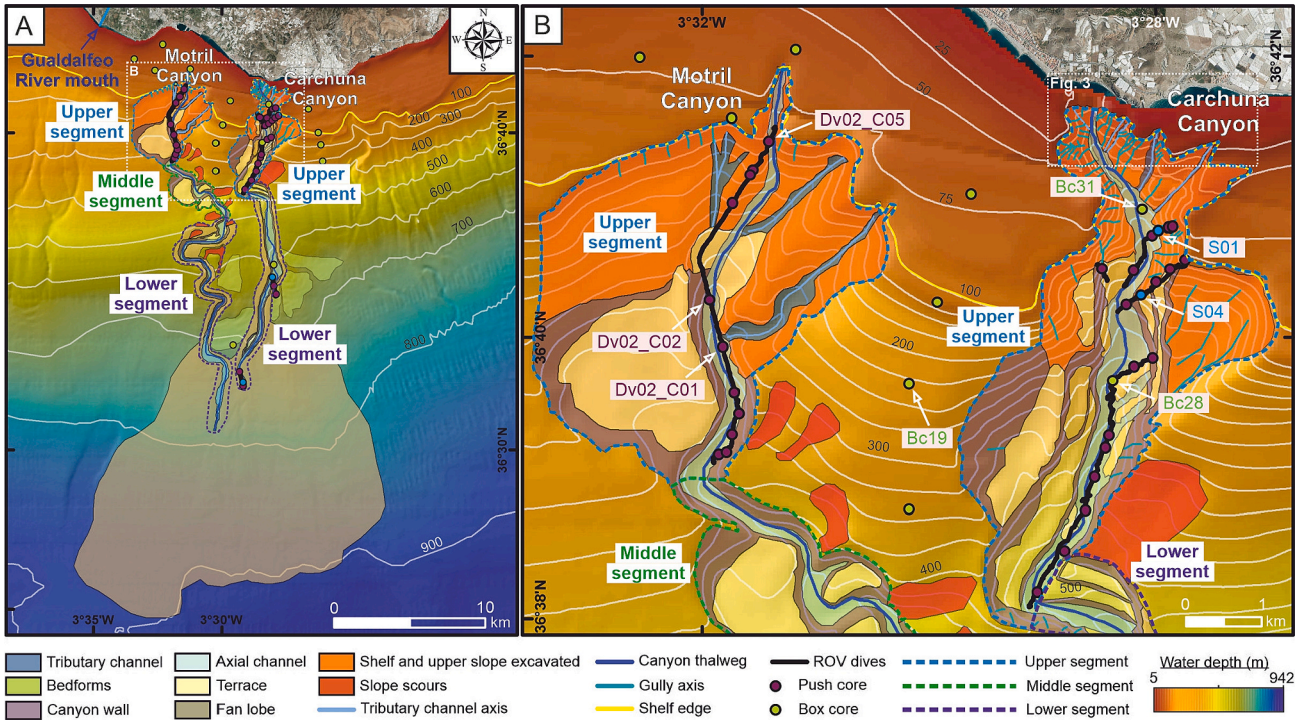

Fig. 2. (A) Geomorphological mapping of the study area and zoom of the shelf and upper slope (B) over the 50 m resolution bathymetric grid, showing the segment distribution within each canyon. Push and box core location and ROV dives executed during ALSSOMAR 2019 survey are also indicated. Bathymetric contours in meters.

Table 2
Main morphological and sedimentological differences between Motril and Carchuna canyons.

		Motril Canyon	Carchuna Canyon
Longitudinal profile		Slightly concave	Very concave
Upper segment	Distance from the coastline	2200 m	200 m
	Close to the river mouth	Yes, Guadalfeo River	No
	Canyon head	4.3 km wide, U-shaped	1.5 km wide, V-shaped
	Tributary channels WF	1 channel 1.1 km long and 180 m wide	2 channels up to 700 m long and 50 m wide. Several 300 m long gullies
	Tributary channels EF	2 channels up to 2.5 km long and up to 200 m wide	3 channels up to 1 km long and 125 m wide. Heads cut IPW. Several 500 m long gullies
	Axial channel	Straight	Straight with bedforms
	Terraces WF	1 terrace with 2500 m wide	Up to 900 m and 150 m wide
	Terraces EF	No	Up to 500 m long and 150 m wide terraces
	Sedimentary facies	Medium silts in AC. Coarse silts in WF	Very fine in canyon head. Coarse silts in AC. Fine sands in WF; Very fine sands in EF
	Organic matter	High in AC. Low in WF	High in the lower reaches. Low in canyon head
	Sediment cores	Massive and homogenous muds	Sandy muds along AC. Sands in flanks
	Mass accumulation rates	15.21 kg·m^2·yr^{-1}; 1.45 cm·yr^{-1}	5.40 kg·m^2·yr^{-1}; 0.49 cm·yr^{-1}
	Surficial foraminifera	Lack of reworked foraminifera downcanyon	Decrease of values of foraminiferal fragments and reworked
Middle segment	Axial channel	Sinuous	
	Terraces WF	2 terraces up to 1.5 km^2 (3.5° slope gradient)	
	Terraces EF	Excavated areas disconnected from the AC (17° slope gradient)	
Lower segment	Axial channel	Meandering, from 900 to 300 m wide	Straight, from 430 to 150 m wide
	Levees	Wide	Narrow
	Superimposed undulations over levee	Yes, NW-SE orientation of the crests	Yes, NW-SE orientation of the crests. Area of 25 km^2
	Sedimentary facies	–	Very fine sands in AC. Coarse silts in eastern levee
	Organic matter	–	High in the termination of the channel
	Sediment cores	–	Muds with interbedded sands along AC
	Surficial foraminifera	–	High percentage of planktonic foraminifera (%P)

WF: Western flank: EF: Eastern flank; IPW: Infralittoral prograding wedge; AC: Axial channel.

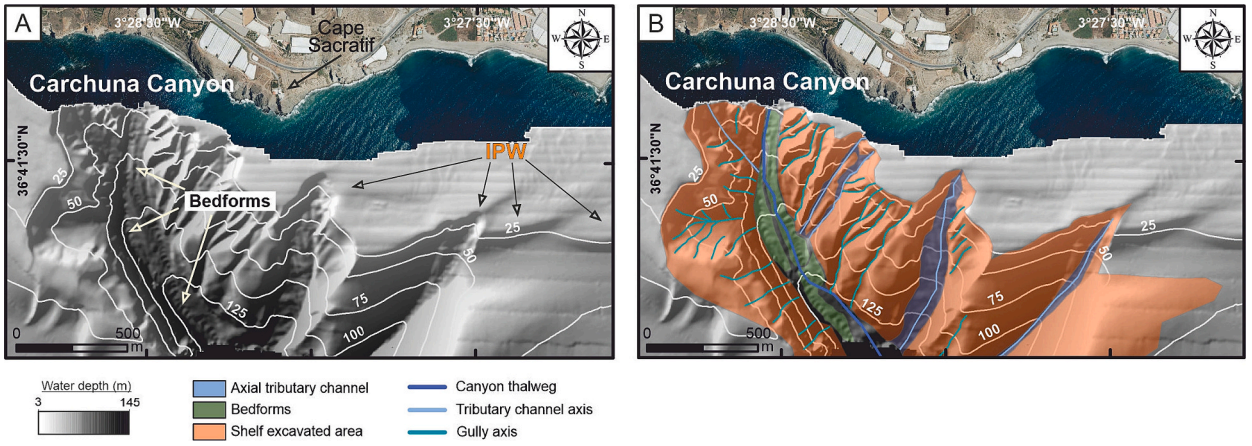

Fig. 3. (A) Shaded relief from a 5 m resolution bathymetric grid (Ministerio de Pesca, Agricultura y Alimentación, 2002) of the Carchuna Canyon head incised in the shelf and cutting the Carchuna Infralittoral Prograding Wedge (IPW). (B) Geomorphological mapping of the Carchuna Canyon head. Bathymetric contours in meters.

has a sinuosity index of 1.28, an average width of 1.5 km, and a maximum width of 4.6 km. The maximum width of the axial channel is 1560 m and its maximum incision is 179 m. The maximum gradient of the canyon walls is ca. 17°. Motril Canyon is fed by 17 gullies (12 in the western and 5 in the eastern flank) mainly located in the upper segment (Table 1). The longitudinal profile of the Motril Canyon thalweg is slightly concave (Fig. 4A). The thalweg profile exhibits four knickpoints located at 110, 210, 450, and 670 m water depths (Fig. 4A). The axial channel is U-shaped, and the flanks locally exhibit terraced features dipping outward from the axial channel (Fig. 4A). In the lower segment, the narrow channel is limited by wide levees (Fig. 4A).

In terms of canyon depth, the relief grows progressively, reaching its highest value (ca. 40 m) at 250 m water depth in the upper segment; after which the relief decreases downslope, showing two peaks in the middle segment, ca. 25 m at 400 m water depth and ca. 20 m at 500 m water depth; and one peak in the lower segment, ca. 15 m at 580 m water depth (Fig. 4B and D). The relief in the canyon head regarding intercanyon depth exhibits high values between 130 and 225 m water depth (Fig. 4B). The canyon gradient has a maximum value of 10° at the shelf edge (Fig. 4B, and D).

Altogether, the values of canyon width, incision, and area decrease from the upper to the lower segment, although canyon width and incision have high values at ca. 2100, 8000, and 11,800 m from the canyon head (Fig. 4C) that correspond to 260, 460, and 610 m water depths, respectively (Fig. 4D). The canyon cross-section area decreases downcanyon, yet exhibits a peak value at 460 m water depth (8 km off the canyon head) that coincides with the change from the middle to the lower segment (Fig. 4C and D).

4.1.2.2. Carchuna Canyon. The Carchuna Canyon, some 20 km long,

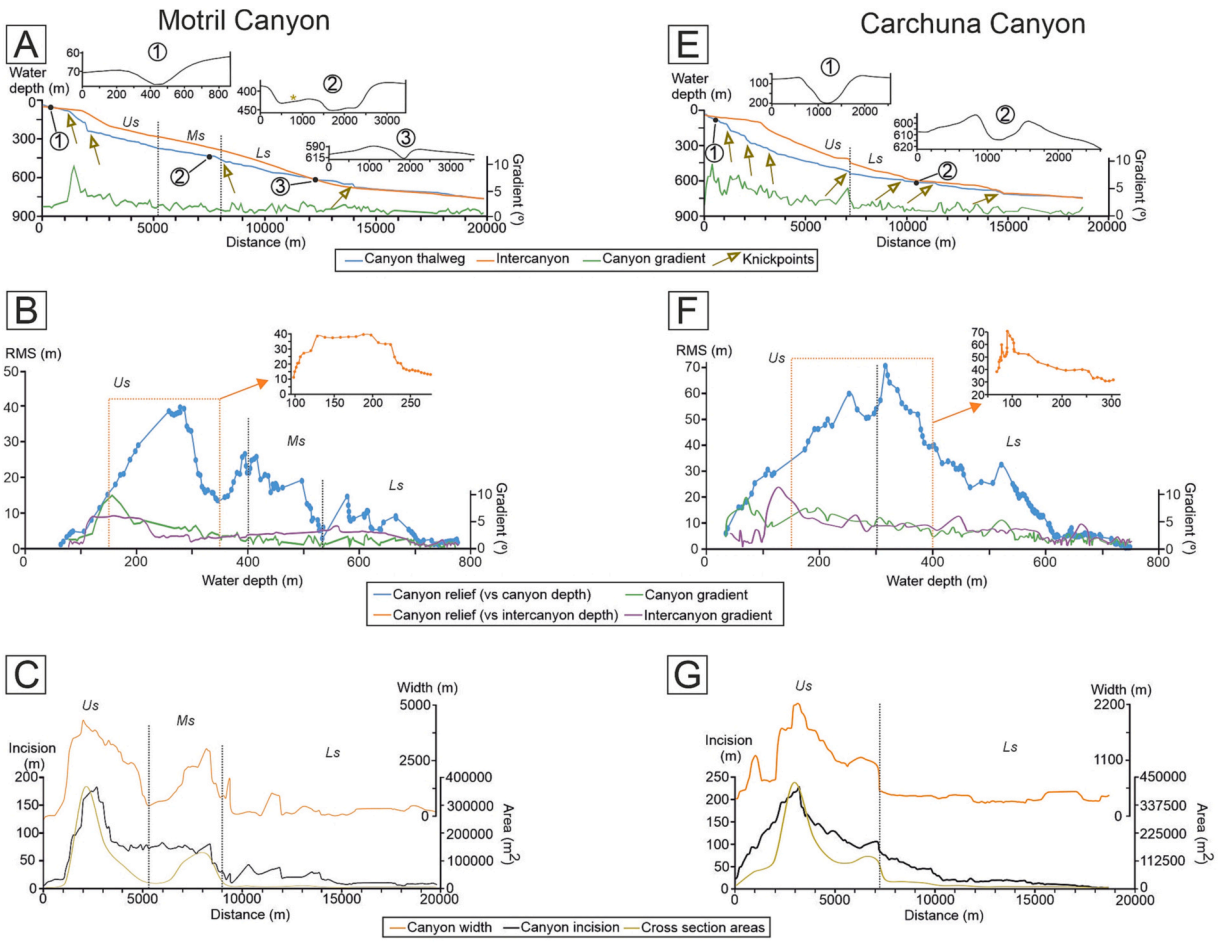

(caption on next page)

Fig. 4. Bathymetric profiles of the Motril and Carchuna canyons, showing the relationships between selected morphologic parameters. (A, E) Depth profiles along the Motril and Carchuna canyons' thalweg (blue line), with indications of knickpoints, and along the intercanyon slope (orange line). The canyon gradient is measured along the canyon thalweg (green line). Transverse profiles of each segment of the both canyons are also shown. The yellow asterisk indicates terraced features dipping outward from the axial channel of the Motril Canyon. (B, F) Downslope variation of canyon relief (vs canyon depth) (blue line), canyon relief (vs intercanyon depth) in the canyon head (orange line), canyon gradient along the Motril and Carchuna canyons (green line), and slope gradient of the intercanyon area (purple line). (C, G) Downslope changes in canyon width (orange line), incision (black line) and cross-sectional area (yellow line) along the Motril and Carchuna canyons. (D, H) Bathymetric grid of the study area showing the canyon thalweg (in white), the intercanyon (in black), and the cross-sections (in blue) used in the Motril and Carchuna canyons (highlighted in green); bathymetric contours in meters. The black dotted line in figs. A-G mark the boundary between the upper (Us), the middle (Ms), and the lower segments (Ls) of the Motril and Carchuna canyons. (For interpretation of the references to colour in this figure legend, the reader is referred to the web version of this article.)

has a sinuosity index of 1.15, an average width of 1.2 km, and a maximum width of 4020 m. The maximum incision is 226 m, the maximum axial channel width is 2160 m, and the maximum gradient of the canyon walls is ca. 34°. Fifty-five gullies are excavated in the flanks, mainly in the upper segment (Table 1).

The longitudinal profile of the Carchuna Canyon thalweg is characterized by a concave up shape (Fig. 4E). Several knickpoints are found in the upper segment. One knickpoint is located in the transition from the upper to the lower segment, at 520 m water depth. Two additional knickpoints lie along the lower segment at 650 and 690 m water depths (Fig. 4E and H). Transversal depth profiles of the Carchuna Canyon show V shapes in the upper segment and U shapes along the lower segment, having narrower levees (Fig. 4E).

Canyon relief values progressively increase up to 70 m in the middle part of the upper segment at 320 m water depth; downslope, canyon relief decreases toward the lower segment, with a peak value of 32 m at the abrupt transition between the upper and lower segments (Fig. 4F and H). The relief in the canyon head with respect to intercanyon depth exhibits a high value at 90 m water depth and then a downcanyon decrease (Fig. 4E). High canyon gradient values are situated along the Carchuna Canyon head (up to 100 m water depth). Although gradient values decrease steadily toward the lower segment, several knickpoints run into high values of canyon gradients along the Carchuna Canyon: e.g., 7° at 180 m water depth, 5° at 300 and 520 m water depths, 2.5° at 650 m water depth, and 2.2° at 690 m water depth (Fig. 4F).

Overall, canyon width, incision, and cross-section values for the Carchuna Canyon decrease with parallel trends from the upper to the lower segment (Fig. 4G and H). High values of canyon width, incision, and area occur at 300 and 490 m water depths. The latter water depth coincides with the upper-lower segment transition. Furthermore, the canyon width exhibits peak values at 100 m water depth in the Carchuna Canyon head (Fig. 4G and H).

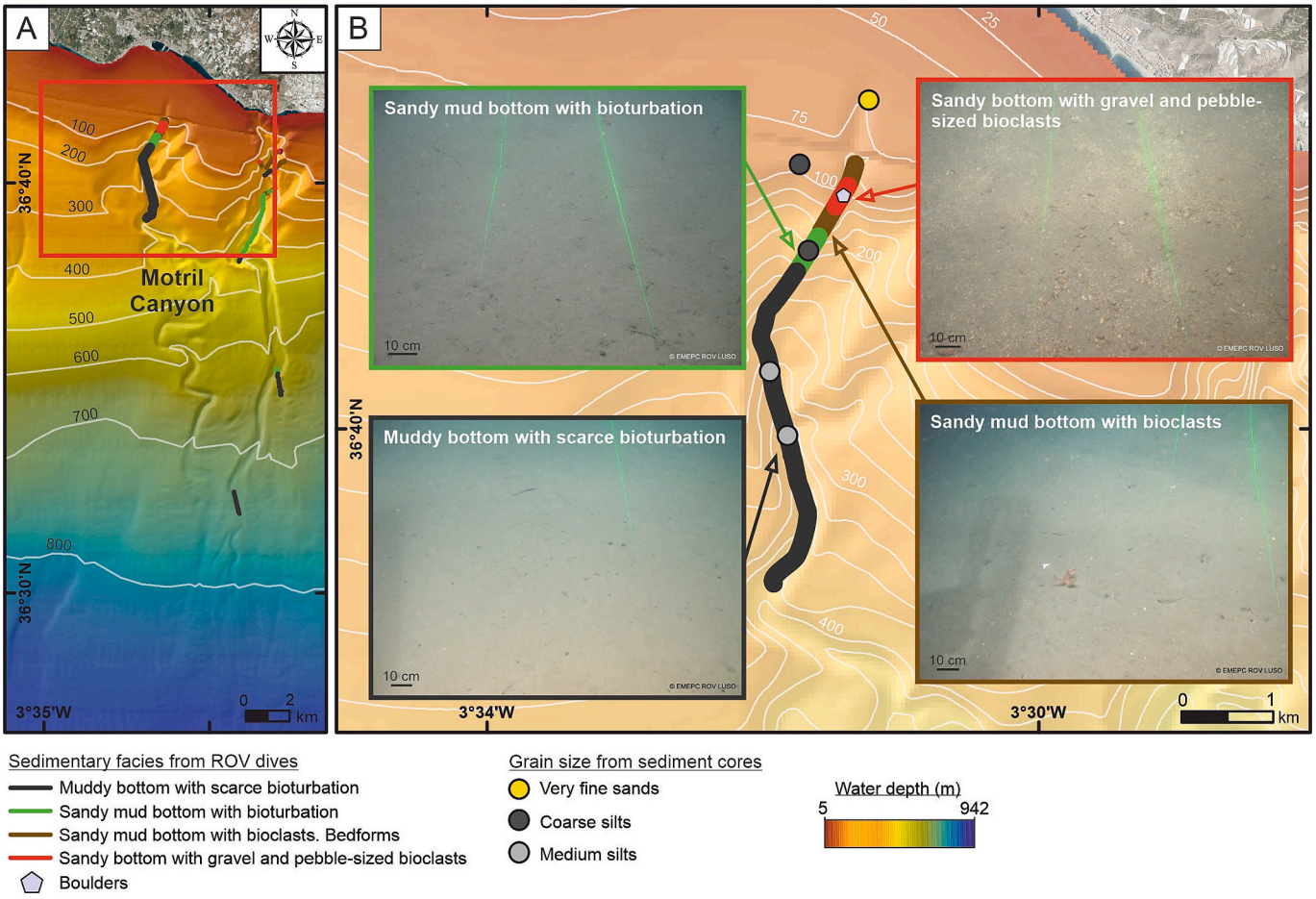

Fig. 5. Sedimentary facies along ROV dives and texture of surficial sediment samples in the Motril Canyon (A) and zoom of specific dive sites with photographic images of representative seafloor sedimentary facies (B). Laser beam spacing of 62 cm. Bathymetric contours in meters.

4.2. Surficial sediments

4.2.1. Sedimentary facies from seafloor imaging and grain size

The seafloor of the upper segment of the Motril Canyon comprises four sedimentary facies (Fig. 5; Table 2). In the shallowest upper segment, the axial channel is characterized by very fine sands that evolve toward the shelf edge to sandy mud including scarce gravel and pebble bioclasts (Fig. 5B). Downcanyon, the axial channel has a homogeneous muddy floor with medium silts and scarce bioturbation (Fig. 5B). Coarser sediments with sandy mud floors showing bioturbation and bioclasts would characterize the western flank of the tributaries (Fig. 5B).

Carchuna Canyon displays six sedimentary facies along its entire length (Fig. 6; Table 2). In the shallowest part of the upper segment, the axial channel exhibits sandy mud floors with bioclasts that evolve downcanyon to sandy muds with coarse silts and bioturbation (Fig. 6B). The eastern flank is characterized by very fine sands with pebble-sized bioclasts and granules, along with cobble clasts, poorly sorted and colonized by bivalves (Fig. 6B). The bioclasts comprise coralline red algae and disarticulated fragmented bivalves. The western flank is characterized by well-sorted fine sands with gravel and pebble-sized coralline red algae (Fig. 6B). The axial channel is characterized by muddy sediments in the transition between the upper and the lower segments (Fig. 6B). In the lower one, the axial channel has sandy mud floors: very fine sands and bioturbation (Fig. 6A). Yet lateral levees in the lower segment can be characterized as homogeneous muddy floors with coarse silts and bioturbation (Fig. 6A).

4.2.2. Organic matter and carbonate contents

The seafloor sediments in the shallowest part of the upper segment of the Motril Canyon have low organic matter (5 %) and carbonate (6 %) contents (Fig. 7A and B). Downcanyon, the axial channel exhibits the highest values of organic matter (ca. 8 %), while carbonate content varies between 5 % and 8 % (Fig. 7A and B; Table 2).

In the upper segment of the Carchuna Canyon, the axial channel reflects a downcanyon increase of organic matter content (from ca. 5 % to 12 %), whereas carbonate content increases slightly, from ca. 5 % to 8 % (Fig. 7A and B; Table 2). The flanks of the upper segment exhibit the lowest content in organic matter (ca. 4 %). Carbonate percentages range between 12 % in the eastern flank to ca. 20 % in the western flank.

In the lower segment of the Carchuna Canyon, organic matter content increases from ca. 7 % to 9 % downcanyon, from the axial channel to the lobe, though carbonate percentages are homogeneous along the axial channel, their values (7–8 %) being similar to those of the upper segment (Fig. 7A and B; Table 2). The highest organic matter and carbonate percentages (up to 10 %) in this segment are found in the eastern levee.

4.3. Sub-surface sediments

4.3.1. Sediment cores

Sediment cores near the Guadalfeo River mouth —at about 50 m water depth— are characterized by sandy mud containing clasts and bioclasts with interbedded fine sands, alongside homogenous mud with organic matter clasts (Fig. 8). The bioclasts are mostly abraded

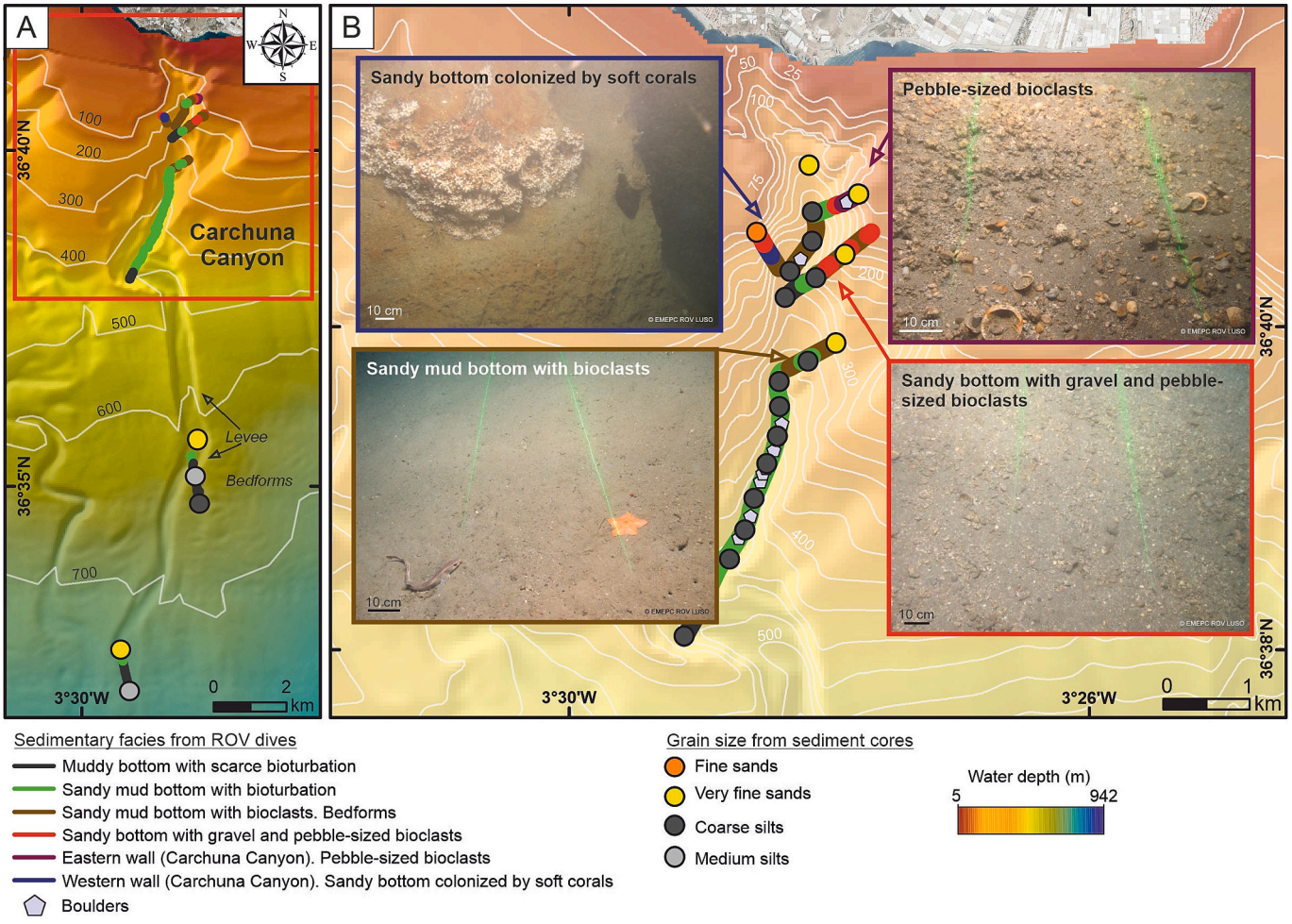

Fig. 6. Sedimentary facies along ROV dives and texture of surficial sediment samples in the Carchuna Canyon (A) and zoom of specific upper segment dive sites with photographic images of representative seafloor sedimentary facies (B). Laser beam spacing of 62 cm. Bathymetric contours in meters.

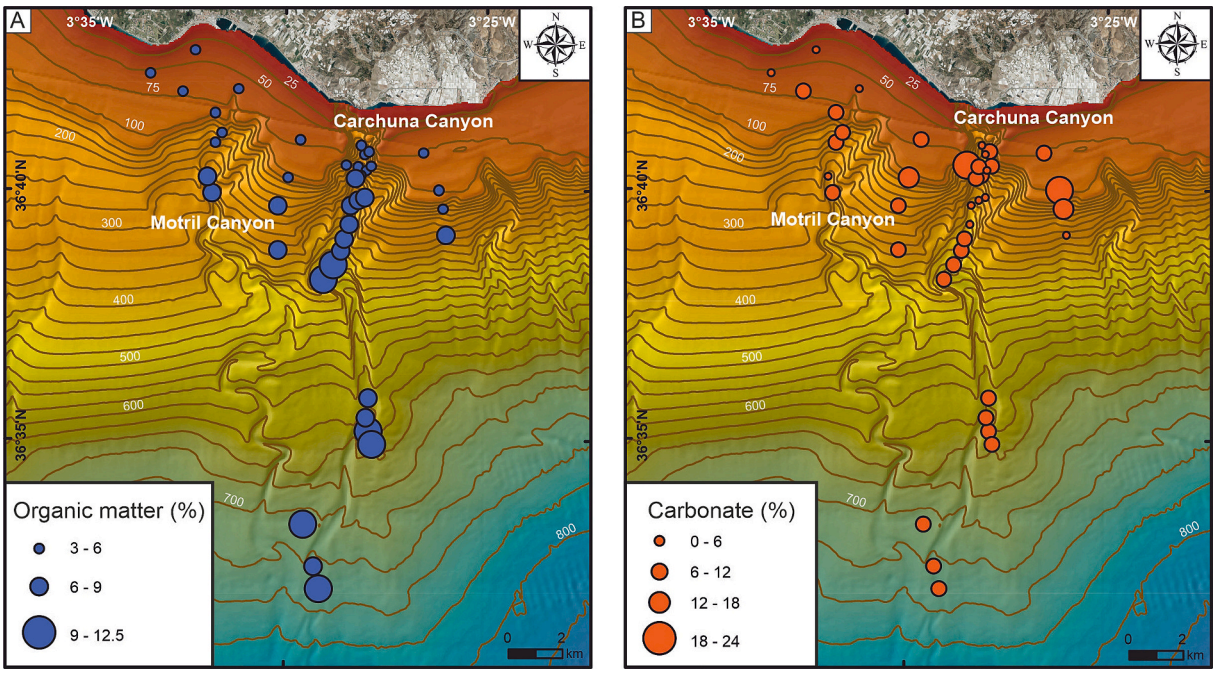

Fig. 7. Percentages of organic matter (A) and carbonate (B) in surficial sediment samples of the study area. Bathymetric contours in meters.

fragmented bivalve shells, whereas the lithoclasts are sub-angular pebbles. Sub-surface sediments along the upper segment of the Motril Canyon are quite homogeneous. They show massive homogeneous mud with negligible percentages of very fine sands. (Fig. 8; Table 2). A fining-upward trend, from coarse and medium sands with sub-rounded bioclasts to sandy muds with a few bioclastic remains, is found in the shallowest sector of the upper segment. These cores are capped by very thin beds with matrix-supported gravels.

Sediment cores along the Carchuna Canyon exhibit a more heterogeneous composition (Fig. 8; Table 2). Sandy muds with bioclasts and interbedded very fine sands are found in the canyon head. Downcanyon, homogenous sandy mud lie over medium and fine sand. The distal part of the upper segment is characterized by massive and homogeneous mud. In both flanks of the upper segment, coarsening-upward trends with sub-rounded very coarse sands, and gravel and pebble-sized bioclasts formed by sub-angular disarticulated shells, can be observed (Fig. 8). Homogeneous sandy muds with very thin interbedded well-sorted fine sands as well as sub-rounded very coarse bioclastic sand and gravel occur along the lower segment axial channel (Fig. 8). Finally, fining-upward trends —from basal sands to homogeneous sandy muds with thin interbedded sands— are discerned in the lateral levees and the distal lobe (Fig. 8).

4.3.2. *Mass accumulation rates*

The highest mass accumulation rate measured in the study area resides in the axial channel of the Motril Canyon (312 m water depth; Fig. 9A and B; Table 2): an average value of 15.21 $kg{\cdot}m^{-2}\ yr^{-1}$, where the sedimentation rate is 1.45 $cm{\cdot}yr^{-1}$. In contrast, the lowest mass accumulation rate (5.40 $kg{\cdot}m^{-2}\ yr^{-1}$) occurs in the axial channel of the Carchuna canyon (370 m water depth; Fig. 9A and C; Table 2), at a sedimentation rate of 0.49 $cm{\cdot}yr^{-1}$. The intercanyon area (230 m water depth; Fig. 9A and D) can be characterized by a mass accumulation rate of 11.13 $kg{\cdot}m^{-2}\ yr^{-1}$ and a sedimentation rate of 0.96 $cm{\cdot}yr^{-1}$.

4.3.3. *Surficial foraminifera*

The percentage of benthic foraminifera in the shallowest part of the upper segment of the Motril Canyon ranges from 61 % to 70 %. These values decrease downcanyon, to 59 % in the upper segment axial channel (Fig. 10). Meanwhile, planktonic foraminifera increase significantly downcanyon from 13 % to 28 % along the axial channel (Fig. 10). The values of foraminiferal fragments are constant (~12 %) along the upper segment of the Motril Canyon (Fig. 10). There is a sharp downslope decrease in the number of reworked foraminifera —from 14 % to 0 %— in the upper segment (Fig. 10; Table 2).

In the Carchuna Canyon, benthic foraminiferal content increases downcanyon in the upper segment, from 66 % to 72 %. However, they become less frequent in the lower segment (31 %) (Fig. 10). Planktonic foraminifera are constant throughout the upper segment (~20 %) and increase toward the lower segment (62 %). The values of foraminiferal fragments decrease downcanyon in both the upper and lower segments —from 9 % to 6 % and from 5 % to 4 %, respectively (Fig. 10). The values of reworked foraminifera decrease downcanyon from 3 % in the canyon head to 1 % in the deeper sector of the upper segment. In the lower segment, the values remain constant, ~3 % (Fig. 10; Table 2).

The lower segment of the Carchuna Canyon has the highest values of transported shelf taxa, which include *Elphidium crispum*, *Ammonia beccarii*, *Elphidium complanatum*, *Quinqueloculina berthelotiana*, *Quinqueloculina pseudobuchiana*, *Elphidium advenum*, *Pseudotriloculina limbata*, *Neoconorbina terquemi* and *Asterigerinata* spp. (Murray, 1991, 2006; Pérez-Asensio and Aguirre, 2010) (Table 3). The flanks of the upper segment exhibit lower values of transported shelf taxa. In turn, the percentage of planktonic foraminifera (%P) exhibits higher values in the lower segment (54.3 % and 72.3 %) than in the upper segment (6.7 % and 37 %) (Tables 2 and 3).

5. Discussion

The first detailed mapping of the Motril and Carchuna canyons reveals substantial geomorphological and sedimentary differences between the two, despite their close proximity. We discuss the relationships between sedimentary processes and canyon morphology, in addition to the implications regarding recent canyon activity.

5.1. *Relation between sedimentary processes and canyon morphology*

5.1.1. *Comparison with other shelf-incised canyons*

The studied canyons show spatial patterns and dimensions that differ from the average population of Mediterranean canyons. The Motril and

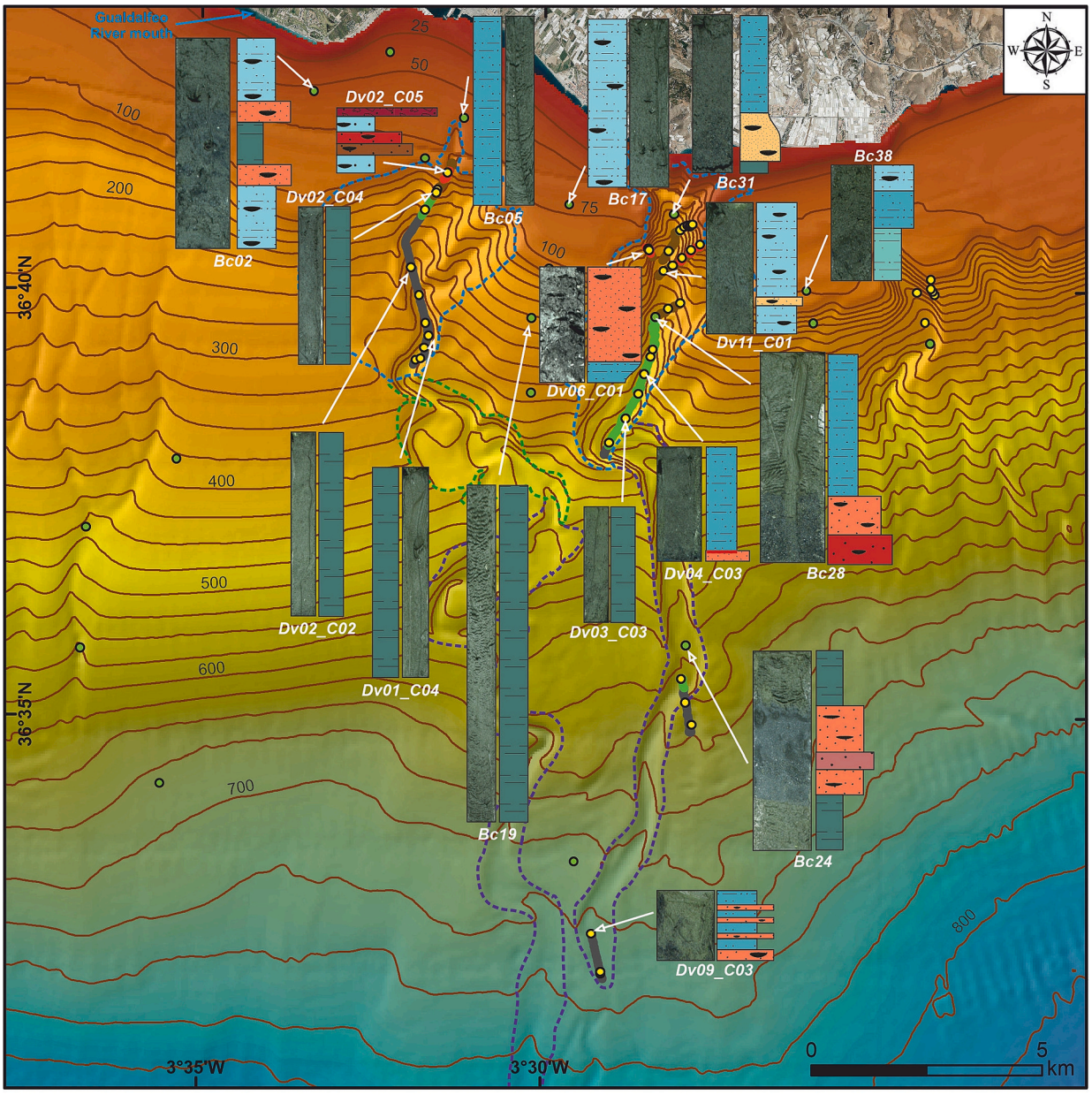

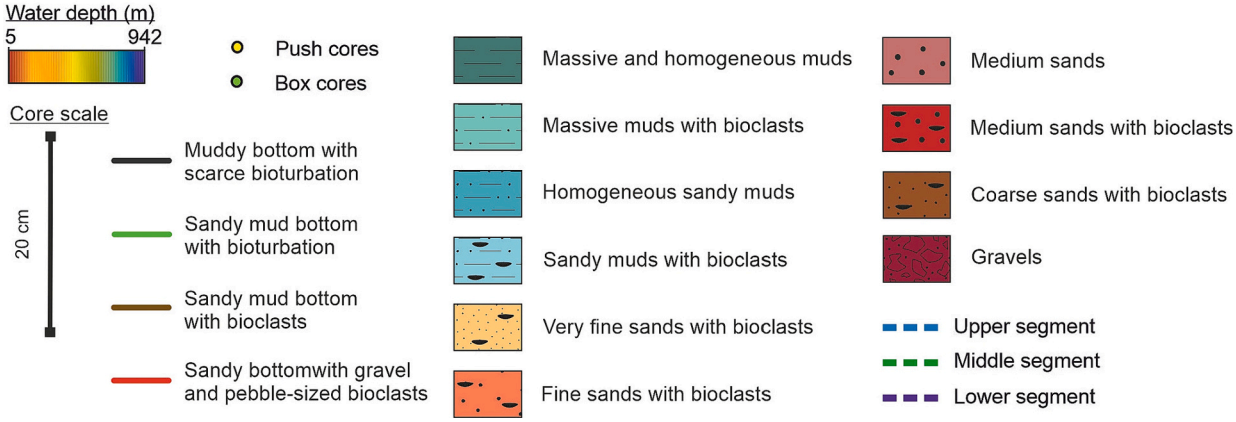

Fig. 8. Sedimentary logs of main short sediment cores (collected with push and box corers) along the studied canyons, the intercanyon area, and the shelf around the study area. The segment distribution within each canyon and surficial sedimentary facies along ROV dives are also indicated. Bathymetric contours in meters.

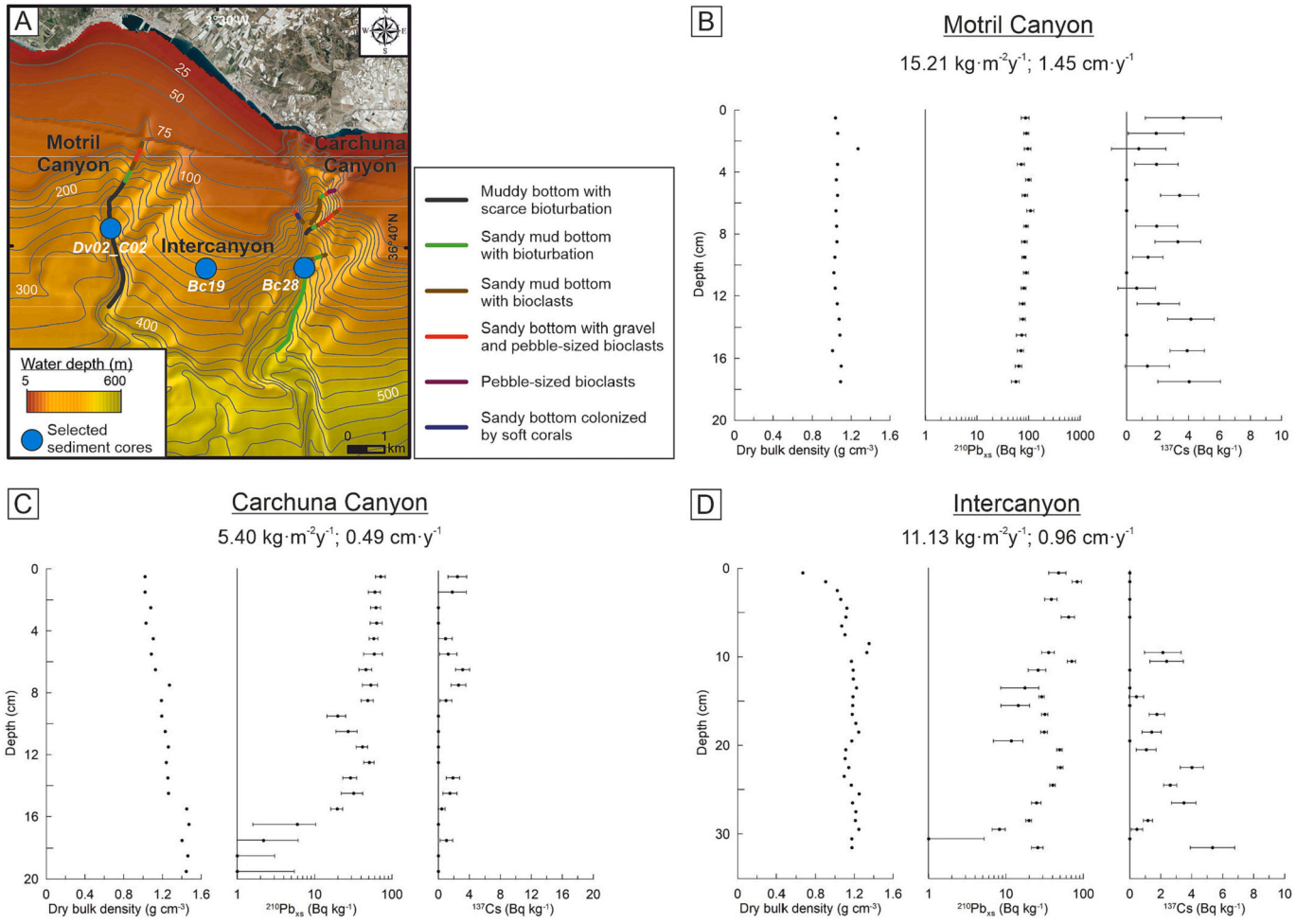

Fig. 9. Dry bulk density and ^{210}Pb and ^{137}Cs activities in three short sediment cores located in the study area (A): Motril Canyon (B), Carchuna Canyon (C), and intercanyon site (D).

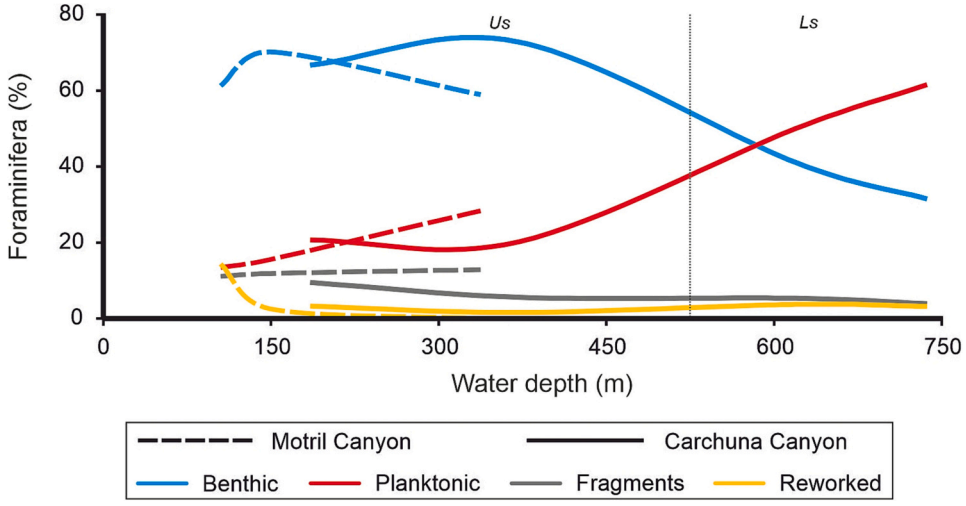

Fig. 10. (A) Percentage of benthic and planktonic foraminifera along the upper segment of the Motril Canyon (dashed lines) and Carchuna Canyon (continuous lines) showing fragments and reworked foraminifera. The black dotted line marks the boundary between the upper (Us) and the lower segments (Ls) of the Carchuna Canyon.

Carchuna canyons are slightly shorter, narrower, less incised, and less steep than Mediterranean canyons (Table 4). These differences point to a lower development of the studied canyons that may be linked to sediment discharges toward the coast and the capture of longshore sediment transport by the canyon heads (Bernhardt and Schwanghart, 2021) considering that the occurrence of shelf-incised Mediterranean canyons correlates with regionally averaged sediment discharge to the coast (Harris and Macmillan-Lawler, 2015). In the study area, the sediment

Table 3
Benthic foraminiferal assemblages of the studied ROV samples located in the Carchuna Canyon showing the percentage of each species (numbers in brackets) and transported shelf taxa in bold. The total percentage of transported shelf taxa, the percentage of planktonic foraminifera (%P), and the sampling water depth for each sample are also indicated. See Fig. 1D for location of the surficial samples.

S01	S02	S03	S04
Lobatula lobatula (34.8)	***Elphidium crispum* (11.2)**	***Elphidium crispum* (18.8)**	*Lobatula lobatula* (11.2)
Cibicides refulgens (16.3)	*Cassidulina laevigata* (10.6)	*Quinqueloculina seminulum* (13.1)	*Cibicides refulgens* (10.3)
Elphidium complanatum (15.7)	*Quinqueloculina seminulum* (7.1)	***Quinqueloculina berthelotiana* (5.4)**	*Cassidulina laevigata* (10.0)
Elphidium crispum (4.4)	***Ammonia beccarii* (6.1)**	***Ammonia beccarii* (5.1)**	***Elphidium complanatum* (10.0)**
Cibicides spp. (3.1)	***Elphidium complanatum* (6.1)**	*Hyalinea balthica* (5.1)	***Elphidium crispum* (5.9)**
Ammonia beccarii (2.2)	***Quinqueloculina berthelotiana* (5.4)**	*Cibicidoides mundulus* (4.8)	*Quinqueloculina seminulum* (5.6)
Quinqueloculina seminulum (1.9)	*Cibicides refulgens* (5.1)	***Quinqueloculina pseudobuchiana* (4.8)**	*Uvigerina peregrina* (5.0)
Lachlanella spp. (1.6)	*Lobatula lobatula* (4.5)	*Cassidulina laevigata* (4.1)	***Nonion faba* (4.4)**
***Quinqueloculina berthelotiana* (1.6)**	*Bolivina spathulata* (3.8)	*Melonis affinis* (2.9)	***Quinqueloculina berthelotiana* (3.7)**
	Quinqueloculina spp. (3.5)	*Uvigerina peregrina* (2.9)	*Trifarina angulosa* (3.4)
	***Elphidium advenum* (3.2)**	*Bulimina marginata* (2.5)	***Ammonia beccarii* (2.8)**
	Bulimina gibba (2.2)	*Cibicides refulgens* (2.5)	***Bulimina elongata* (2.8)**
	Cibicidoides mundulus (1.9)	***Elphidium complanatum* (2.5)**	*Bolivina spathulata* (2.5)
	Hyalinea balthica (1.9)	*Lobatula lobatula* (2.2)	*Spiroplectinella wrighti* (2.2)
	Melonis affinis (1.9)	***Pseudotriloculina limbata* (2.2)**	***Asterigerinata mamilla* (1.9)**
	***Neoconorbina terquemi* (1.9)**	*Hoeglundina elegans* (1.9)	
	Triloculina tricarinata (1.6)	***Asterigerinata* spp. (1.6)**	
		Cibicidoides wuellerstorfi (1.6)	
		Triloculina tricarinata (1.6)	
Total transported shelf taxa (%): 5.0	Total transported shelf taxa (%): 48.7	Total transported shelf taxa (%): 45.5	Total transported shelf taxa (%): 39.3
%P: 6.7	%P: 54.3	%P: 72.3	%P: 37.0
Sampling depth (m): 149	Sampling depth (m): 741	Sampling depth (m): 633	Sampling depth (m): 261

discharged from the rivers is vastly smaller than Mediterranean canyons (Table 4). Modern canyon head connectivity with the coast has been proposed for the Carchuna Canyon, which likely captures littoral drift cells (Ortega-Sánchez et al., 2014). In the case of the Motril Canyon, its head incised in the shelf could eventually constitute a limited collector of south-eastward derived sediment plumes emanating from the Guadalfeo River mouth (Lobo et al., 2006; Bárcenas et al., 2011).

In addition, shelf-sourced canyons have a range of sedimentary features and processes that reflect downslope changes in canyon geometry, signaling a transition from proximal erosive to distal depositional settings (e.g., Lastras et al., 2009; Brothers et al., 2013). The studied canyons generally meet these observations, both exhibiting proximal incisions flanked by tributary channels and gullies. Distally, the lower segments of both canyons show U-shaped axial channels with

Table 4
Differences in the spatial patterns and dimensions between the studied canyons and the Mediterranean canyons.

Main characteristics	Motril and Carchuna canyons	Mediterranean canyons (mean)
Length	27 and 20 km	ca. 30 km (Harris et al., 2014)
Width	4.6 and 4 km	ca. 8 km (Harris and Macmillan-Lawler, 2015)
Incision	792 and 741 m	ca. 1100 m (Harris et al., 2014)
Slope gradient	ca. 2.3°	ca. 6.5° (Harris and Whiteway, 2011)
Rivers associated	Guadalfeo River, up to ca. 24 $m^3 \cdot s^{-1}$ (Bárcenas et al., 2015)	Gulf of Lion, ca. 2000 $m^3 \cdot s^{-1}$ (e.g., Palanques et al., 2012); Catalan Coast, ca. 400 $m^3 \cdot s^{-1}$ (e.g., Tubau et al., 2015)
Channel-levee length	ca. 11 km	Alboran canyons, ca. 4 km e.g., Ercilla et al., 2019; Rest of canyons, >15 km (e.g., Gamberi et al., 2013)

lateral levees and superimposed bedforms, as evidenced in other Mediterranean canyons (e.g., Cap de Creus Canyon, Lastras et al., 2007; Neto-Lipuda Canyon, Rebesco et al., 2009). The depositional features of the Motril and Carchuna canyons are similar to those of other shelf-incised canyons systems around the Alboran Sea (e.g., the Guadiaro Canyon, Alonso and Ercilla, 2002a, 2002b), but their channel-levee systems are longer than other Alboran Sea canyons and shorter than other Mediterranean canyons (Table 4). Shorter channel-levee systems in the Mediterranean Sea can be attributed either to the absence of connection between canyon heads and river mouths, or to the presence of short rivers near canyon heads that mainly supply coarse-grained sediment; this appears to be the case along the northern Alboran Sea and the Catalan Coast.

Despite general similarities, the Motril and Carchuna canyons also exhibit distinctive features not often found in canyon populations. One outstanding trait is the occurrence of straight segments of variable orientations, which is generally associated with fault control on canyon geometry (e.g., Popescu et al., 2004; García et al., 2006; Gaudin et al., 2006). The Motril and Carchuna canyons share an abrupt change (ca. 90°) in the orientation of the axial channel in the upper segment termination (Fig. 2). This most likely indicates tectonic control in the WNW-ESE orientation of the Motril and Carchuna axial channels, due to a normal fault that crosses both sectors (Fig. 1C) (Comas et al., 1999; Pérez-Belzuz, 1999; Rodriguez et al., 2017) that may also condition the variations observed in canyon relief, incision, and area (Fig. 4), suggesting that erosional and/or depositional processes are enhanced in segment transitions. The termination of the segments, related to abrupt orientation changes of the axial channels, would favor the deposition of muddy sediments and wider canyon sections as observed in both canyons (Figs. 4, 5, 6, and 8). In the segment of the axial channel having WNW-ESE orientation, associated with tectonic control (Figs. 1C and 2B), the values of canyon relief and incision are high (Fig. 4B, C, F, and G), suggesting a dominance of erosional processes along both canyons. The abrupt change of the axial channel from WNW-ESE to N-S in both canyons accompanies canyon widening (Fig. 4C and G) and subsequent sediment deposition in the lateral levees (Fig. 2A).

Overall, shelf-incised canyons tend to exhibit downslope increases in canyon width (e.g., Chiang and Yu, 2006; Lastras et al., 2007, 2009; Gamboa et al., 2012; Wiles et al., 2019), while canyon relief decreases downcanyon (e.g., Goff, 2001; Baztan et al., 2005; Green et al., 2007; Puga-Bernabéu et al., 2013; Micallef et al., 2014; Wiles et al., 2019). Such general trends are attributed to the dominance of erosional processes upslope, including retrogressive failures (Goff, 2001; Green et al., 2007; Li et al., 2021; Li et al., 2023). In other cases, heightened downcanyon relief may result from greater erosion or the convergence of abundant canyon tributaries (Goff, 2001). Although the relief, width, incision, and cross-section area values of the Motril and Carchuna

canyons are concordant among themselves and decrease downcanyon (Fig. 4), the variation of one parameter with respect to the others may evidence erosive or depositional sectors controlled by local factors. Specifically, abrupt orientation changes of the axial channel in both submarine canyons condition variations in canyon relief, incision, and area along their traces. Noteworthy on the one hand are the shelf incision of the Carchuna Canyon and its proximity to the coast, showing a high width value at 120 m water depth (Fig. 4G). In turn, the Motril Canyon exhibits low relief (Fig. 4B) and high width at 350 m water depth in the upper segment (Fig. 4C), suggesting a depositional area; and high relief (Fig. 4B) and low width and incision (Fig. 4C) at 500 m water depth, in coincidence with an abrupt change of the axial channel, in the middle to lower segment transition.

5.1.2. Geomorphological differences between Motril and Carchuna canyons

In spite of their close proximity and the fact that they share some common geomorphological attributes, the Motril and Carchuna canyons also exhibit striking differences that could hold implications for the distinct dominance of sedimentary processes in each canyon setting.

The shapes of longitudinal depth profiles along submarine canyons provide information about the balance between sediment supply and transport (Gerber et al., 2009; Covault et al., 2011). A concave thalweg downslope profile is interpreted to signal the modification of the original slope shape by erosional processes in the canyon head and the deposit of transported material at the termination of the channel (Mitchell, 2005; Gerber et al., 2009; Kertznus and Kneller, 2009; Covault et al., 2011; Amblas et al., 2012). Very concave profiles are linked to canyons that are relatively steep in their proximal reaches having coarse-grained sediments and being incised in narrow shelves (Covault et al., 2011). In contrast, the slightly concave shape of submarine canyons is associated with fine-grained sediments and wide, mature passive continental margins (Covault et al., 2011). Although the Motril and Carchuna canyons are located in a narrow margin nearby high topography hinterlands, they exhibit different grades of concave longitudinal profiles, hence indicative of different equilibrium states (Fig. 4). In addition, the longitudinal profile of the Motril Canyon is also slightly divergent from concave profiles of other canyons (Covault et al., 2011) (Fig. 11). Thus, the tectonic setting or the individual physiographic parameters of each canyon do not suffice to explain the evolution of the submarine canyon; several factors intervene, meaning a detailed study is needed.

The very concave shape and occurrence of sandy muds along the Carchuna Canyon axial channel (Figs. 4, 6 and 8) point to a continuous supply of sandy sediments, regardless of the sea-level stand (Covault et al., 2011). Such profiles are indicative of significant bypass of the canyon head as it distally feeds downslope turbidity currents (Gerber et al., 2009). The Carchuna Canyon furthermore shows conspicuous evidence of erosional activity (Lastras et al., 2011), such as higher incision depths and the occurrence of knickpoints (Fig. 4). In contrast, the dominance of muddy sediments along the axial channel of the Motril Canyon (Figs. 5 and 8), and the sigmoidal shape of the intercanyon area (Fig. 4A) could be attributed to an excess of sediment supplied by the Guadalfeo River mouth in the upper reaches of the Motril Canyon and shelf, as evidenced elsewhere, where submarine canyons may serve as mud traps collecting sediments exchanged between river mouths and offshore (e.g., Prins et al., 2000; Liu et al., 2002; Walsh and Nittrouer, 2003; Hill et al., 2009; Clift et al., 2014; Warrick, 2014). In fact, upper slope sigmoidal profiles have been linked to sediment supply exceeding the capacity of subaqueous currents to transport sediments downslope (e.g., Gerber et al., 2009; Amblas et al., 2012; Puga-Bernabéu et al., 2013; Soutter et al., 2021). Differences between the recent erosional/depositional behavior of the two canyons studied are also seen in the canyon relief values (Fig. 4): low for the Motril Canyon, likely due to a more recent depositional setting; high for the Carchuna Canyon, indicating significant erosional processes.

The two canyons exhibit different sinuosity values as well (Table 1). The Motril Canyon shows a meandering path downslope and distal axial channel narrowing (Fig. 2), an overall pattern accompanied by a low gradient (Fig. 4) and mantling with fine-grained sediments (Fig. 5). In contrast, the Carchuna Canyon is straighter, steeper and floored by coarser sediments (Figs. 2, 4 and 6). Yet both overlie similar features of

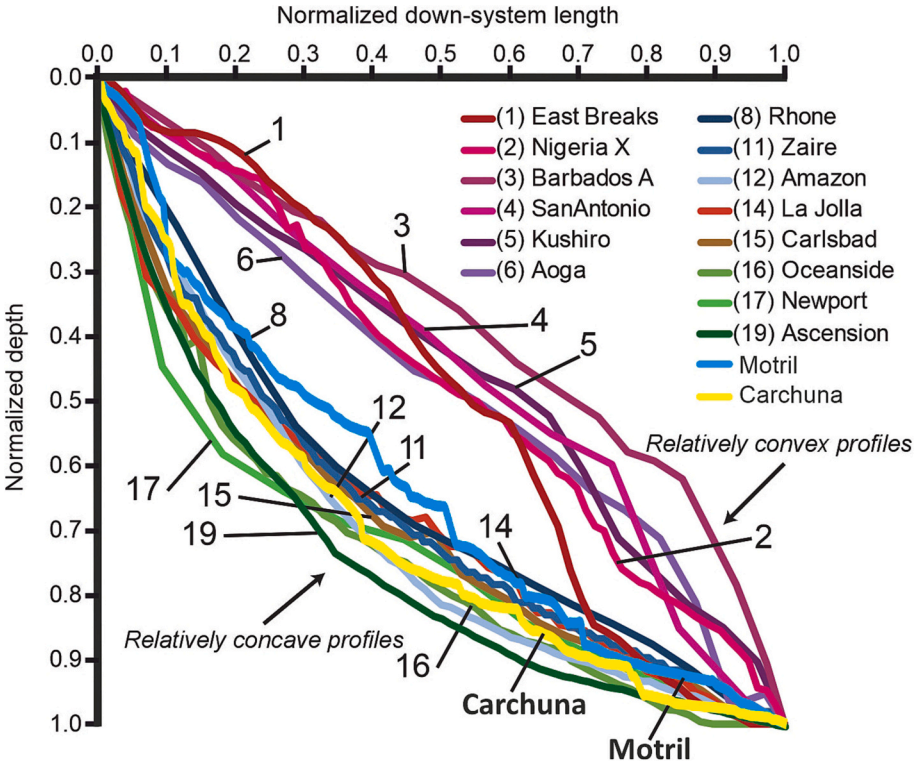

Fig. 11. Canyon longitudinal profiles normalized on the basis of profile lengths (from canyon head to the end of the confined portion of the system) of nineteen submarine canyons and the two studied canyons (after Covault et al., 2011).

the gradient slope. Therefore, the sinuosity differences point to different phases of maturity (Clark et al., 1992; Kane et al., 2008; Babonneau et al., 2010; Janocko et al., 2013; Wiles et al., 2019), even if both studied canyons exhibit contrasting recent activities, as it will be discussed in the following section.

The greater sinuosity of the Motril Canyon would indicate a more mature state, an interpretation supported by the wide terraces along the upper and middle segments (Fig. 2) indicative of lateral canyon migrations (Clark et al., 1992; Mayall et al., 2006; Arzola et al., 2008) and interpreted as generated through progressive erosion, channel migration, and meander development, as documented in other canyon systems (e.g., Babonneau et al., 2010; Hubbard et al., 2014; Jobe et al., 2015). At some sites the terraces dip away from the axial channel (Fig. 4A), a morphological configuration indicative of sediment aggradation in the boundary of the channel by sediment overflows (Babonneau et al., 2004). In addition, the dominance of fined-grained sediments that mantle the axial channel is also related to low gradient, highly sinuous canyons (e.g., Abreu et al., 2003). In line with this interpretation, the less sinuous, steeper, and coarser-grained Carchuna Canyon would be related to a youthful development, possibly associated with the erosive behavior of coarse-grained turbidity currents (Clark et al., 1992; Clark and Pickering, 1996). In addition, its narrow, elongated terraces at various depths (Fig. 2) may evidence multiple axial incisions (Baztan et al., 2005; Arzola et al., 2008; Micallef et al., 2014), or even recent canyon excavation (Tubau et al., 2013).

Finally, another distinctive or contrasting feature is that the two canyons have very different canyon heads, in terms of morphology and sediment composition. Canyon heads contribute to the erosion and deepening of upper canyons that bypass the slope via canyon valleys, reshaping canyon walls through widening and shelf incision and increasing material delivery into the axial channel (Pratson and Coakley, 1996; Popescu et al., 2004; Puga-Bernabéu et al., 2011; Micallef et al., 2014; Li et al., 2021; Li et al., 2023).

The deep shelf incision of the Carchuna Canyon can be attributed to canyon head widening along the shelf edge, and penetration farther into the shelf toward the coastline over time. Headward erosion is also evidenced by the high values of canyon relief (vs intercanyon depth) upslope from the shelf edge (Fig. 4F), indicating retrogression of the canyon head (Green et al., 2007). The strong entrenchment of the thalweg of the Carchuna Canyon head limits its lateral migration, impeding the creation of terraces, while producing the erosion of the walls and terraces, as evidenced by the occurrence of gullies and steep flanks (Figs. 2 and 3). Besides, the abundance of bioclasts and coarse-grained sizes are compatible with widespread sediment failures distally evolving into turbidity flows. Indeed, the V-shaped canyon head is characteristic of turbidity-flow dominated canyons (Babonneau et al., 2004; Rebesco et al., 2009; Li et al., 2021; Li et al., 2023).

In marked contrast, in the Motril Canyon, the high values of canyon relief (vs intercanyon depth) are recorded downcanyon of the shelf edge (Fig. 4B), meaning that the canyon head widened mostly along the shelf edge over time (Green et al., 2007). The lack of entrenchment of the thalweg is evidenced by the cross-profiles that exhibit U shapes in the upper reaches of the canyon (Fig. 4A), and the finer-grained sediment composition. Therefore, the above would indicate minor mass movements from the canyon head to the axial channel (Babonneau et al., 2004; Rebesco et al., 2009), and partial mantling by hemipelagic deposition.

5.2. Implications for canyon activity

Many canyons presently active, and capable of maintaining their levels of activity during sea-level highstands, do not directly depend on sediment input from a river or river mouth (e.g., the Cap de Creus Canyon, Canals et al., 2006; the Monterey Canyon, Xu et al., 2008; Heijnen et al., 2022). In fact, the volume of sediment deposited in shallow water that might be captured by canyons relies on two factors (Mullenbach and Nittrouer, 2000; Puig et al., 2014, 2017; Sweet and Blum, 2016): the degree of canyon shelf incision and the location of the canyon head with respect to the main sedimentary source (Herzer and Lewis, 1979; Mullenbach et al., 2004; Green, 2009; Bernhardt et al., 2015; Bernhardt and Schwanghart, 2021).

The distance between the canyon head and the shoreline strongly conditions sediment transport. Shelf-incised canyons are able to capture either transported shelf sediments, water masses potentially transporting sediments, or deep-sea currents (e.g., Canals et al., 2006; Marchès et al., 2007; Xu et al., 2008). Shelf-incised canyons can additionally be distinguished according to the principal sedimentary source supplying the canyon heads: longshore-drift-fed systems, river-fed systems, or delta-fed systems (Sweet and Blum, 2016). The fact that the Motril and Carchuna canyons exhibit significant geomorphological and sedimentary differences suggests they played distinct roles in recent patterns of sediment transport and accumulation, hence displaying diverse degrees of canyon shelf incision. The Motril Canyon head lies ca. 2 km from the coastline and close to the Guadalfeo River mouth; whereas the Carchuna Canyon head is 200 m offshore and cuts infralittoral prograding wedges (Figs. 2 and 3).

Although the Motril Canyon exhibits a mature state, there are strong indications that at present the Motril Canyon accumulates sediment along the axial channel and acts as a sediment trap. The dominance of muddy sediments (Figs. 5 and 8) and high values of organic matter (Fig. 7A) point to fine sediment settling with low sediment remobilization in submarine canyons (Cronin et al., 2005; Oliveira et al., 2007) where the heads are remote to the shoreline and show low activity (Harris and Whiteway, 2011; Sweet and Blum, 2016; Mascle et al., 2015). The lack of sediment transport through the Motril Canyon axial channel is further supported by a lack of shelf benthic foraminifera transported along the channel (Fig. 10). In addition, sedimentation and mass accumulation rates (1.45 $cm \cdot yr^{-1}$ and 15.21 $kg \cdot m^{-2}\ yr^{-1}$; Fig. 9B) are higher than in other western Mediterranean submarine canyons, where accumulation rates do not exceed 0.47 $cm \cdot yr^{-1}$ (Miralles et al., 2005; Martín et al., 2008; Puig et al., 2008; Zúñiga et al., 2009). Low densities of marine litter buried and scattered along the Motril Canyon also agrees with its recent behavior as a sediment sink (Cerrillo-Escoriza et al., 2023).

Contrariwise, the Carchuna Canyon is envisaged as an active system whose canyon head is able to capture littoral cell sediments, eventually leading to sediment transport along the axial channel toward the channel termination owing to turbidity flows. Longshore sheltering and wave focusing in canyon heads are known to lead to increased shear stress that can mobilize coarse-grained sediments (Smith et al., 2018). This interpretation is supported by several lines of evidence. In the upper segment, the bedforms superposed over the tributary channels located in the eastern flank and the axial channel of the Carchuna Canyon head (Figs. 2B and 3) evidence downcanyon sediment transport from the tributary channels to the axial channel, and from the axial channel of the canyon head to the downcanyon. In addition, active canyon heads tend to be located in the vicinity of shorelines, and are mantled by coarse-grained sediments (e.g., Lewis and Barnes, 1999; Mullenbach and Nittrouer, 2000; Normandeau et al., 2015; Sweet and Blum, 2016). In the Carchuna Canyon, the coarse composition of surficial sediments located in the axial channel (Figs. 6 and 8), the lower mass sediment accumulation rates in comparison with the Motril Canyon and the intercanyon area (Fig. 9), and the high values of organic matter found in the termination of the upper segment (Fig. 7A), are indicative of transport by turbidity flows, as in other canyons (e.g., Biscara et al., 2011). Further support of the occurrence of deep transport by turbidity flows along the Carchuna Canyon is provided by the accumulations of marine litter in the upper segment, in turn favored by the irregular morphology dictated by rocky seafloor areas and smooth depressions along the thalweg (Cerrillo-Escoriza et al., 2023).

Within the lower segment of the Carchuna Canyon, the coarser surficial sediment samples (Fig. 6) and the high values of organic matter

(Fig. 7A) found along the axial channel suggest sediment transport, whereas the sediment waves superimposed over the eastern levee (Fig. 2) signal overflow. Similar values for carbonate contents along the Carchuna Canyon (Fig. 7B) support that the sediment along the axial channel is uniform and predominantly terrigenous, without significant variations due to shelf bioclastic or pelagic contributions (Puga-Bernabéu et al., 2011). Coarse-grained sediment transport most likely reached the distal termination of the channel, as evidenced by the occurrence of sub-surface interbedded sands (Fig. 8), high values of organic matter (Fig. 7A), and high values of transported shelf benthic foraminifera (Table 3); all these evidences are indicative of transported material (Schmiedl et al., 2000; Bolliet et al., 2014; Duros et al., 2014).

The differences in sediment trapping and downcanyon transport efficiency highlighted above can be explained by the physiographic configuration of each canyon, plus their interaction with wind-driven regional oceanographic conditions. Two basic situations are envisaged, given the seasonal alternance of wind regimes. Under westerlies dominance, shelf currents trend toward the E-SE (Bárcenas et al., 2011; Fig. 12A), when the Motril Canyon head can capture laterally redistributed fine-grained sediments supplied by the Guadalfeo River (Fig. 12A and C). In the Carchuna Canyon head, energetic western waves mainly influence the eastern flank (Ortega-Sánchez et al., 2014); this process is reflected in the submarine geomorphology of the head, as the eastern flank shows widespread erosional features. Enhanced erosion of the eastern flank may resuspend sediments by the canyon head, ultimately favoring the formation of sediment transport pulses driven by downcanyon bottom flows, as described in the bottom layer (Serrano et al., 2020; Fig. 12C).

Canyon activity would be more limited under easterlies dominance. For one, sediment erosion and remobilization would have been reduced in the Carchuna canyon head, as eastern waves are less energetic (Ortega-Sánchez et al., 2014). Yet canyon activity cannot be discarded during such conditions: W-NW directed shelf currents exhibit velocities above 0.1 $m \cdot s^{-1}$ (Bárcenas et al., 2011; Fig. 12B), conditions that could trigger the input of moderate amounts of sediments in the canyon, subsequently redistributed downslope by downwelling flows, likewise active during easterlies dominance (Serrano et al., 2020; Fig. 12D). In contrast, the Motril Canyon would essentially be inactive under

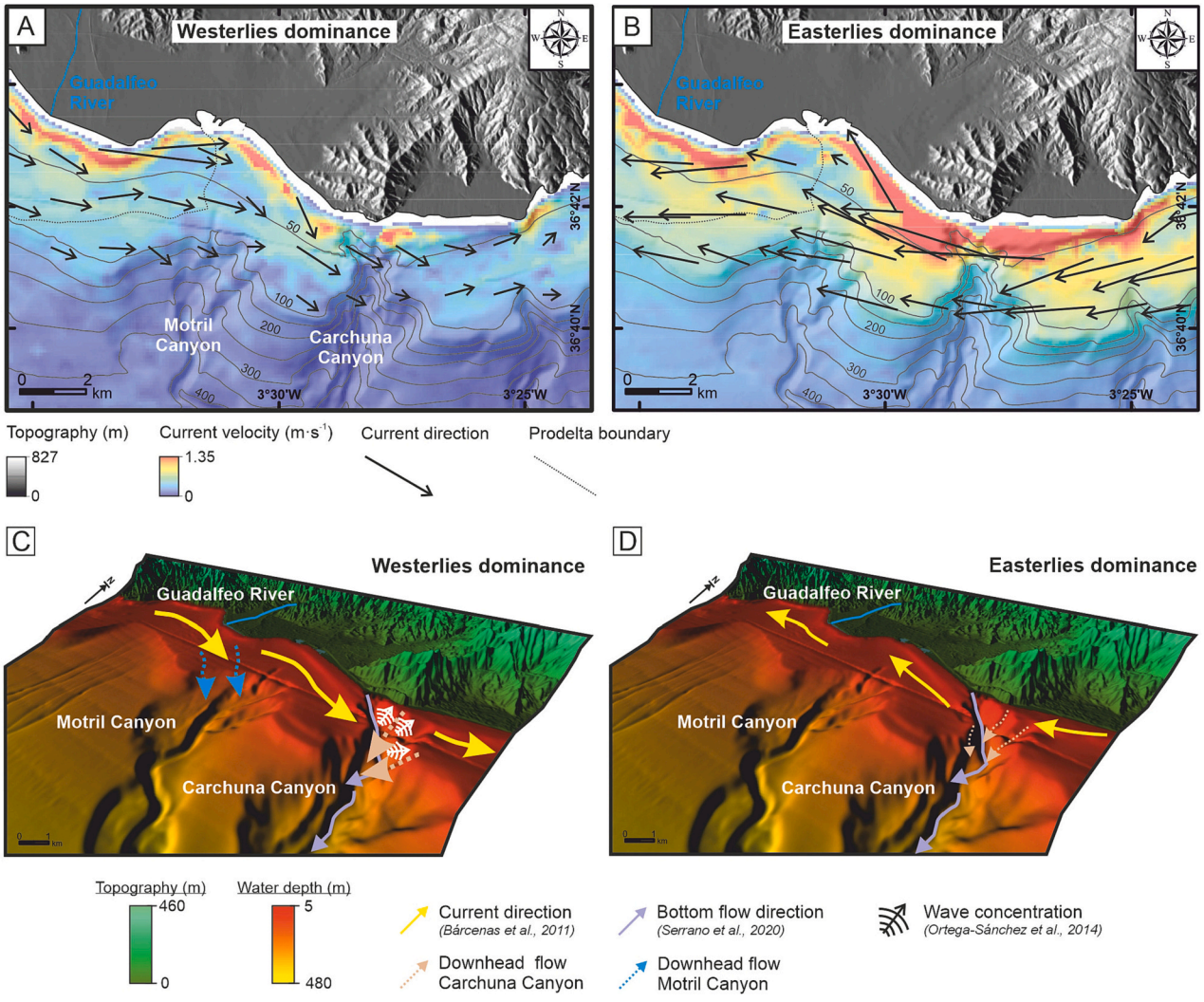

Fig. 12. Mapping of direction and depth-averaged current speed ($m \cdot s^{-1}$) under westerlies dominance (A) and easterlies dominance (B) (modified from Bárcenas et al., 2011). The black dotted line indicates the prodelta boundary (extracted from Lobo et al., 2015). Bathymetric contours in meters. Model of recent sedimentary activity in the upper segments of the Motril and Carchuna canyons based on the current direction (Bárcenas et al., 2011), bottom flow direction (Serrano et al., 2020), and wave concentration in the Carchuna Canyon head (Ortega-Sánchez et al., 2014). Under westerlies dominance (C), the Motril Canyon head receives fine sediments supplied by the lateral redistribution of the Guadalfeo River input, whereas energetic western waves erode the eastern flank of the Carchuna Canyon head, feeding downcanyon sediment transport pulses. Under easterlies dominance (D), wave activity is reduced in the Carchuna Canyon head, although the canyon may intercept limited sediment transport by relatively intense shelf currents; in contrast, the Motril Canyon head remains essentially inactive.

easterlies dominance, because of the trapping effect of the Carchuna Canyon —impeding westward-directed sediment flows— and the minor influence of Guadalfeo River inputs.

6. Conclusions

Although the Motril and Carchuna canyons share morphologic features typical of Mediterranean canyons, they also exhibit a number of distinctive features. They have segments characterized by downslope variations of geomorphological parameters attributed to enhanced erosional/depositional processes and promoted by tectonically controlled abrupt changes of the axial channel orientation.

Significant geomorphological differences between the two studied canyons reflect different balances between canyon maturity and recent activity of sedimentary processes. The U-shaped Motril Canyon head suggests the imprint of minor mass movements in the canyon head that jointly with the greater sinuosity, the occurrence of wide terraces, the low slope gradients, and the slightly concave shape point to a relatively mature system. In contrast, the steeper Carchuna Canyon with the deep V-shaped incision of the canyon head, the less sinuosity, the coarser-grained sediments along the axial channel, and the narrow and elongated terraces would be related to a youthful canyon development.

The degree of shelf incision, the location of the Motril and Carchuna canyon heads in relation with the local sediment sources, and the seasonally variable hydrodynamic regimes determine the amount of sediment potentially captured by both canyons and hence, the recent sedimentary activity. In the recent past, the Motril Canyon has mainly acted as a sediment trap accumulating hemipelagic sediments, where the distant location of the canyon head from the coastline (ca. 2 km) favors fine-grained sediment accumulation from the major regional fluvial source, mainly under wind-driven westerlies dominance. In contrast, the proximity of the Carchuna Canyon to the coastline (<200 m) favors littoral cell sediment trapping, under both wind-driven westerlies and easterlies dominance, downslope coarse-grained sediment transport and continuous thalweg erosion driven by turbidity flows along the axial channel toward the channel termination.

CRediT authorship contribution statement

J. Cerrillo-Escoriza: Writing – review & editing, Writing – original draft, Visualization, Validation, Methodology, Investigation, Formal analysis, Data curation, Conceptualization. **F.J. Lobo:** Validation, Supervision, Software, Resources, Project administration, Funding acquisition, Data curation, Conceptualization. **Á. Puga-Bernabéu:** Validation, Supervision, Methodology, Investigation, Conceptualization, Data curation. **P. Bárcenas:** Validation, Methodology, Formal analysis, Data curation. **I. Mendes:** Validation, Software, Methodology, Formal analysis. **J.N. Pérez-Asensio:** Validation, Methodology, Formal analysis, Data curation. **R. Durán:** Validation, Supervision, Methodology, Investigation, Data curation. **T.J. Andersen:** Methodology, Formal analysis, Data curation. **Á. Carrión-Torrente:** Visualization, Validation, Methodology. **M. García:** Visualization, Validation, Methodology, Investigation. **A. López-Quirós:** Visualization, Validation, Methodology. **M. Luján:** Visualization, Validation, Methodology. **A. Mena:** Visualization, Validation, Methodology. **O. Sánchez-Guillamón:** Visualization, Validation, Methodology, Formal analysis. **M.J. Sánchez:** Visualization, Validation, Methodology, Formal analysis.

Declaration of competing interest

The authors declare that they have no known competing financial interests or personal relationships that could have appeared to influence the work reported in this paper.

Data availability

Data will be made available on request.

Acknowledgements

This research was executed in the framework of the following projects: Alboran Shelf-Slope cOupling processes and deep sediMent trAnsfeR: Source To Sink approaches and implications for biodiversity–ALSSOMAR S2S (CTM2017-88237-P), funded by "Ministerio de Economía y Competitividad", Spanish government, and Sediment gravity flows and ANthropogenic Impacts in a MEDiterranean deltaic-and-canyon environment: Causal relationships and consequences–SANIMED (PID2021-125489OB-I00) funded by MCIN/AEI/10.13039/501100011033/FEDER, UE. This study is also part of Cerrillo-Escoriza's PhD project, supported by Grant PRE2018-084812 funded by MCIN/AEI/10.13039/501100011033 and FSE "Invierte en tu future". The authors wish to thank the captain and crew of R/V Sarmiento de Gamboa for their dedication and constant support for the execution of activities onboard, and to the participants of the ALSSOMAR-S2S expedition for their help during data acquisition. I.M. acknowledges to Fundação para a Ciência e a Tecnologia for Research Assistant contracts DL57/2016/CP1361/CT0009, CEECINST/00052/2021/CP2792/CT0012 and projects UID/0350/2020 CIMA, LA/P/0069/2020ARNET. A.L.Q. is grateful for funding provided by FJC2021-047046-I (MCIN/AEI/10.13039/501100 011033 and NextGenerationEU/PRTR). Jean Sanders conducted an extensive review of the English style of the manuscript. We thank to the guest editor Zhongyuan Chen, to Michele Rebesco and to an anonymous reviewer for helpful and constructive comments and suggestions that greatly improved the quality of the manuscript.

References

Abreu, V., Sullivan, M., Pirmez, C., Mohrig, D., 2003. Lateral accretion packages (LAPs): an important reservoir element in deep water sinuous channels. Mar. Pet. Geol. 20, 631–648. https://doi.org/10.1016/j.marpetgeo.2003.08.003.

Aldaya, F., 1981. Mapa Geológico y Memoria Explicativa de la Hoja 1056 (Albuñol) del Mapa Geológico de España. IGME, Madrid.

Aldaya, F., García-Dueñas, V., Navarro-Vilá, F., 1979. Los Mantos Alpujárrides del tercio central de las Cordilleras Béticas. Ensayo de la correlación tectónica de los Alpujárrides. Acta Geol. Hisp. 14 (1), 154–166.

Alonso, B., Ercilla, G., 2002a. Architecture of modern turbidite systems in different geologic settings on the Spanish margins (NW and SW Mediterranean Sea). In: Briand, F. (Ed.), Turbidite Systems and Deep-Sea Fans of the Mediterranean and the Black Seas. CIESM, Monaco, pp. 19–22.

Alonso, B., Ercilla, G., 2002b. Small turbidite systems in a complex tectonic setting (SW Mediterranean Sea): Morphology and growth patterns. Mar. Pet. Geol. 19 (10), 1225–1240. https://doi.org/10.1016/S0264-8172(03)00036-9.

Amblas, D., Gerber, T.P., De Mol, B., Urgeles, R., Garcia-Castellanos, D., Canals, M., Pratson, L.F., Robb, N., Canning, J., 2012. Survival of a submarine canyon during long-term outbuilding of a continental margin. Geology 40 (6), 543–546. https://doi.org/10.1130/G33178.1.

Amblas, D., Ceramicola, S., Gerber, T.P., Canals, M., Chiocci, F.L., Dowdeswell, J.A., Harris, P.T., Huvenne, V.A.I., Lai, S.Y.J., Lastras, G., Iacono, C. Lo, Micallef, A., Mountjoy, J.J., Paull, C.K., Puig, P., Sanchez-Vidal, A., 2018. Submarine Canyons and Gullies. In: Micallef, A., Krastel, S., Savini, A. (Eds.), Submarine Geomorphology. Springer Geol. Springer, Cham, pp. 251–272. https://doi.org/10.1007/978-3-319-57852-1_14.

Andersen, T.J., 2017. Some practical considerations regarding the application of 210^{Pb} and 137^{Cs} dating to estuarine sediments. In: Weckström, K., Saunders, K., Gell, P., Skilbeck, C. (Eds.), Applications of Paleoenvironmental Techniques in Estuarine Studies, Developments in Paleoenvironmental Research, 20. Springer, Dordrecht, pp. 121–140. https://doi.org/10.1007/978-94-024-0990-1_6.

Appleby, P.G., 2001. Chronostratigraphic techniques in recent sediments. In: Last, W.M., Smol, J.P. (Eds.), Tracking Environmental Change Using Lake Sediments, Developments in Paleoenvironmental Research, vol. 1. Springer, Dordrecht, pp. 171–203. https://doi.org/10.1007/0-306-47669-X_9.

Appleby, P.G., Oldfield, F., 1978. The calculation of lead-210 dates assuming a constant rate of supply of unsupported ^{210}Pb to the sediment. Catena 5 (1), 1–8. https://doi.org/10.1016/S0341-8162(78)80002-2.

Arzola, R.G., Wynn, R.B., Lastras, G., Masson, D.G., Weaver, P.P.E., 2008. Sedimentary features and processes in the Nazaré and Setúbal submarine canyons, west Iberian margin. Mar. Geol. 250 (1–2), 64–88. https://doi.org/10.1016/j.margeo.2007.12.006.

Babonneau, N., Savoye, B., Cremer, M., Klein, B., 2002. Morphology and architecture of the present canyon and channel system of the Zaire deep-sea fan. Mar. Pet. Geol. 19 (4), 445–467. https://doi.org/10.1016/S0264-8172(02)00009-0.

Babonneau, N., Savoye, B., Cremer, M., Bez, M., 2004. Multiple terraces within the deep incised Zaire Valley (ZaïAngo Project): are they confined levees? Geol. Soc. Spec. Publ. 222 (1), 91–114. https://doi.org/10.1144/GSL.SP.2004.222.01.06.

Babonneau, N., Cremer, M., Bez, M., 2010. Sedimentary architecture in meanders of a submarine channel: Detailed study of the present Congo turbidite channel (zaiango project). J. Sediment. Res. 80 (10), 852–866. https://doi.org/10.2110/jsr.2010.078.

Ballesteros, M., Rivera, J., Muñoz, A., Muñoz-Martín, A., Acosta, J., Carbó, A., Uchupi, E., 2008. Alboran Basin, southern Spain-Part II: Neogene tectonic implications for the orogenic float model. Mar. Pet. Geol. 25 (1), 75–101. https://doi.org/10.1016/j.marpetgeo.2007.05.004.

Bárcenas, P., 2013. Procesos Morfogenéticos y Evolución Reciente de los Depósitos Prodeltaicos del Sureste de la Península Ibérica: aplicaciones de Modelos Matemáticos. Ph.D. Thesis Doctoral,. University of Malaga, Malaga, Spain.

Bárcenas, P., Lobo, F.J., Macías, J., Fernández-Salas, L.M., Díaz del Río, V., 2011. Spatial variability of surficial sediments on the northern shelf of the Alboran Sea: the effects of hydrodynamic forcing and supply of sediment by rivers. J. Iber. Geol. 37 (2), 195–214. https://doi.org/10.5209/rev_JIGE.2011.v37.n2.8.

Bárcenas, P., Lobo, F.J., Macías, J., Fernández-Salas, L.M., López-González, N., Díaz del Río, V., 2015. Submarine deltaic geometries linked to steep, mountainous drainage basins in the northern shelf of the Alboran Sea: filling the gaps in the spectrum of deltaic deposition. Geomorphology 232, 125–144. https://doi.org/10.1016/j.geomorph.2014.11.028.

Baztan, J., Berné, S., Olivet, J.L., Rabineau, M., Aslanian, D., Gaudin, M., Réhault, J.P., Canals, M., 2005. Axial incision: the key to understand submarine canyon evolution (in the western Gulf of Lion). Mar. Pet. Geol. 22 (6–7), 805–826. https://doi.org/10.1016/j.marpetgeo.2005.03.011.

Bengtsson, L., Enell, M., 1986. Chemical analysis. In: Berglund, B.E. (Ed.), Handbook of Holocene Palaeoecology and Paleohydrology, vol. 4. Wiley, New York, pp. 423–455. https://doi.org/10.1002/gea.3340040208.

Bernhardt, A., Schwanghart, W., 2021. Where and why do submarine canyons remain connected to the shore during sea-level rise? Insights from global topographic analysis and Bayesian regression. Geophys. Res. Lett. 48 (10), e2020GL092234 https://doi.org/10.1029/2020GL092234.

Bernhardt, A., Melnick, D., Jara-Muñoz, J., Argandoña, B., González, J., Strecker, M.R., 2015. Controls on submarine canyon activity during sea-level highstands: the Biobío canyon system offshore Chile. Geosphere 11, 1226–1255. https://doi.org/10.1130/GES01063.1.

Biscara, L., Mulder, T., Martinez, P., Baudin, F., Etcheber, H., Jouanneau, J.M., Garlan, T., 2011. Transport of terrestrial organic matter in the Ogooué deep sea turbidite system (Gabon). Mar. Pet. Geol. 28 (5), 1061–1072. https://doi.org/10.1016/j.marpetgeo.2010.12.002.

Bolliet, T., Jorissen, F.J., Schmidt, S., Howa, H., 2014. Benthic foraminifera from Cap Breton Canyon revisited; faunal evolution after repetitive sediment disturbance. Deep-Sea Res. II 104, 319–334. https://doi.org/10.1016/j.dsr2.2013.09.009.

Bozzano, G., Alonso, B., Ercilla, G., Estrada, F., García, M., 2009. Late Pleistocene and Holocene Depositional Facies of the Almeria Channel (Alboran Sea, Western Mediterranean). Extern. Control. Deep. Depos. Syst. 92, 199–206. https://doi.org/10.2110/sepmsp.092.199.

Brankart, J.M., Pinardi, N., 2001. Abrupt cooling of the Mediterranean levantine intermediate water at the beginning of the 1980s: Observational evidence and model simulations. J. Phys. Oceanogr. 31 (8), 2307–2320. https://doi.org/10.1175/1520-0485(2001)031<2307:acotml>2.0.co;2.

Brothers, D.S., Brink, U.S., Andrews, B.D., Chaytor, J.D., 2013. Geomorphic characterization of the U.S. Atlantic continental margin. Mar. Geol. 338, 46–63. https://doi.org/10.1016/j.margeo.2012.12.008.

Canals, M., Casamor, J.L., Lastras, G., Monaco, A., Acosta, J., Berné, S., Loubrieu, B., Weaver, P.P.E., Grehan, A., Dennielou, B., 2004. The role of canyons in strata formation. Oceanography 17 (4), 80–91. https://doi.org/10.5670/oceanog.2004.06.

Canals, M., Puig, P., De Madron, X.D., Heussner, S., Palanques, A., Fabres, J., 2006. Flushing submarine canyons. Nature 444, 354–357. https://doi.org/10.1038/nature05271.

Cerrillo-Escoriza, J.L.F., Puga-Bernabéu, Á., Rueda, J.L., Bárcenas, P., Sánchez-Guillamón, O., Serna Quintero, J.M., Pérez Gil, J.L., Murillo, Y., Caballero-Herrera, J.A., López-Quirós, A., Mendes, I., Pérez Asensio, J.N., 2023. Origin and driving mechanisms of marine litter in the shelf- incised Motril, Carchuna, and Calahonda canyons (northern Alboran Sea). Front. Mar. Sci. 10, 1–24. https://doi.org/10.3389/fmars.2023.1098927.

Chiang, C.S., Yu, H.S., 2006. Morphotectonics and incision of the Kaoping submarine canyon. SW Taiwan orogenic wedge. Geomorphology 80 (3–4), 199–213. https://doi.org/10.1016/j.geomorph.2006.02.008.

Clark, J., Kenyon, N., Pickering, K., 1992. Quantitative analysis of the geometry of submarine levees. Geology 20, 633–636. https://doi.org/10.1130/0091-7613(1992)020<0633.

Clark, J.D., Pickering, K.T., 1996. Architectural elements and growth patterns of submarine channels: Application to hydrocarbon exploration. Am. Assoc. Pet. Geol. Bull. 80 (2), 194–221. https://doi.org/10.1306/64ed878c-1724-11d7-8645000102c1865d.

Clift, P.D., Giosan, L., Henstock, T.J., Tabrez, A.R., 2014. Sediment storage and reworking on the shelf and in the Canyon of the Indus River-Fan System since the last glacial maximum. Basin Res. 26 (1), 183–202. https://doi.org/10.1111/bre.12041.

Comas, M.C., García-Dueñas, V., Jurado, M.J., 1992. Neogene tectonic evolution of the Alboran Sea from MCS data. Geo-Mar. Lett. 12 (2–3), 157–164. https://doi.org/10.1007/2FBF02084927.

Comas, M.C., Platt, J.P., Soto, J.I., Watts, A.B., 1999. The origin and tectonic history of the Alboran Basin: Insights from Leg 161 results. Proc. Ocean Drill. Program Sci. Results 161, 555–580. https://doi.org/10.2973/odp.proc.sr.161.262.1999.

Covault, J.A., Fildani, A., Romans, B.W., McHargue, T., 2011. The natural range of submarine canyon-and-channel longitudinal profiles. Geosphere 7 (2), 313–332. https://doi.org/10.1130/GES00610.1.

Cronin, B.T., Akhmetzhanov, A.M., Mazzini, A., Akhmanov, G., Ivanov, M., Kenyon, N. H., 2005. Morphology, evolution and fill: Implications for sand and mud distribution in filling deep-water canyons and slope channel complexes. Sediment. Geol. 179 (1–2), 71–97. https://doi.org/10.1016/j.sedgeo.2005.04.013.

Daly, R.A., 1936. Origin of submarine “canyons”. Am. J. Sci. 31, 401–420. https://doi.org/10.2475/ajs.s5-31.186.401.

Dean Jr., W.E., 1974. Determination of carbonate and organic matter in calcareous sediments and sedimentary rocks by loss on ignition: Comparison with other methods. J. Sediment. Petrol. 44, 242–248. https://doi.org/10.1306/74D729D2-2B21-11D7-8648000102C1865D.

DeGeest, A.L., Mullenbach, B.L., Puig, P., Nittrouer, C.A., Drexler, T.M., Durrieu de Madron, X., Orange, D.L., 2008. Sediment accumulation in the western Gulf of Lions, France: the role of Cap de Creus Canyon in linking shelf and slope sediment dispersal systems. Cont. Shelf Res. 28 (15), 2031–2047. https://doi.org/10.1016/j.csr.2008.02.008.

Drexler, T.M., Nittrouer, C.A., Mullenbach, B.L., 2006. Impact for local morphology on sedimentation in a submarine canyon, ROV studies in Eel Canyon, Northern California, U.S.A. J. Sediment. Res. 76 (5–6), 839–853. https://doi.org/10.2110/jsr.2006.064.

Duros, P., Jorissen, F.J., Cesbron, F., Zaragosi, S., Schmidt, S., Metzger, E., Fontanier, C., 2014. Benthic foraminiferal thanatocoenoses from the Cap-Ferret Canyon area (NE Atlantic): a complex interplay between hydro-sedimentary and biological processes. Deep. Res. Part II Top. Stud. Oceanogr. 104, 145–163. https://doi.org/10.1016/j.dsr2.2013.09.024.

Ercilla, G., Alonso, B., Baraza, J., 1992. Sedimentary evolution of the northwestern Alboran Sea during the Quaternary. Geo-Mar. Lett. 12 (2–3), 144–149. https://doi.org/10.1007/BF02084925.

Ercilla, G., Alonso, B., Baraza, J., 1994. Post-Calabrian sequence stratigraphy of the northwestern Alboran Sea (southwestern Mediterranean). Mar. Geol. 120 (3–4), 249–265. https://doi.org/10.1016/0025-3227(94)90061-2.

Ercilla, G., Juan, C., Hernández-Molina, F.J., Bruno, M., Estrada, F., Alonso, B., Casas, D., Farran, M. Li, Llave, E., García, M., Vázquez, J.T., D'Acremont, E., Gorini, C., Palomino, D., Valencia, J., El Moumni, B., Ammar, A., 2016. Significance of bottom currents in deep-sea morphodynamics: an example from the Alboran Sea. Mar. Geol. 378, 157–170. https://doi.org/10.1016/j.margeo.2015.09.007.

Ercilla, G., Juan, C., Periáñez, R., Alonso, B., Abril, J.M., Estrada, F., Casas, D., Vázquez, J.T., d'Acremont, E., Gorini, C., El Moumni, B., Do Couto, D., Valencia, J., 2019. Influence of along slope processes on modern turbidite systems and canyons in the Alboran Sea (southwestern Mediterranean). Deep. Res. Part I Oceanogr. Res. Pap. 144, 1–16. https://doi.org/10.1016/j.dsr.2018.12.002.

Estrada, F., Ercilla, G., Alonso, B., 1997. Pliocene-Quaternary tectonic-sedimentary evolution of the NE Alboran Sea (SW Mediterranean Sea). Tectonophysics 282 (1–4), 423–442. https://doi.org/10.1016/S0040-1951(97)00227-8.

Fabres, J., Calafat, A., Sanchez-Vidal, A., Canals, M., Heussner, S., 2002. Composition and spatio-temporal variability of particle fluxes in the Western Alboran Gyre, Mediterranean Sea. J. Mar. Syst. 33–34, 431–456. https://doi.org/10.1016/S0924-7963(02)00070-2.

Fernández-Salas, L.M., Dabrio, C.J., Goy, J.L., Díaz del Río, V., Zazo, C., Lobo, F.J., Sanz, J.L., Lario, J., 2009. Land-sea correlation between late Holocene coastal and infralittoral deposits in the SE Iberian Peninsula (Western Mediterranean). Geomorphology 104 (1–2), 4–11. https://doi.org/10.1016/j.geomorph.2008.05.013.

Fisher, W.L., Galloway, W.E., Steel, R.J., Olariu, C., Kerans, C., Mohrig, D., 2021. Deep-water depositional systems supplied by shelf-incising submarine canyons: Recognition and significance in the geologic record. Earth Sci. Rev. 214, 103531 https://doi.org/10.1016/j.earscirev.2021.103531.

Folk, R.L., 1954. The distinction between grain size and mineral composition in sedimentary rock nomenclature. J. Geol. 62 (4), 344–359. https://doi.org/10.1086/626171.

Folk, R.L., Ward, W.C., 1957. Brazos River bar: a study in the significance of grain size parameters. J. Sediment. Petrol. 27 (1), 3–26. https://doi.org/10.1306/74D70646-2B21-11D7-8648000102C1865D.

Frey-Martinez, J., Cartwright, J.A., Burgess, P.M., Bravo, J.V., 2004. 3D seismic interpretation of the Messinian unconformity in the Valencia, Spain. In: Davies, R.J., Cartwright, J.A., Stewart, S.A., Lappin, M., Underhill, R. (Eds.), 3D Seismic Technology: Application to the Exploration of Sedimentary Basins. Geol Soc. Mem., London, pp. 91–100. https://doi.org/10.1144/GSL.MEM.2004.029.01.10.

Gamberi, F., Rovere, M., Dykstra, M., Kane, I.A., Kneller, B.C., 2013. Integrating modern seafloor and outcrop data in the analysis of slope channel architecture and fill. Mar. Pet. Geol. 41 (1), 83–103. https://doi.org/10.1016/j.marpetgeo.2012.04.002.

Gamberi, F., Breda, A., Mellere, D., 2017. Depositional canyon heads at the edge of narrow and tectonically steepened continental shelves: comparing geomorphic elements, processes and facies in modern and outcrop examples. Mar. Pet. Geol. 87, 157–170. https://doi.org/10.1016/j.marpetgeo.2017.06.007.

Gamboa, D., Alves, T.M., Cartwright, J., 2012. A submarine channel confluence classification for topographically confined slopes. Mar. Pet. Geol. 35 (1), 176–189. https://doi.org/10.1016/j.marpetgeo.2012.02.011.

García, M., Alonso, B., Ercilla, G., Gràcia, E., 2006. The tributary valley systems of the Almeria Canyon (Alboran Sea, SW Mediterranean): Sedimentary architecture. Mar. Geol. 226 (3–4), 207–223. https://doi.org/10.1016/j.margeo.2005.10.002.

García-Dueñas, V., Balanyá, J.C., Martínez-Martínez, J.M., 1992. Miocene extensional detachments in the outcropping basement of the northern Alboran Basin (Betics) and their tectonic implications. Geo-Mar. Lett. 12 (2–3), 88–95. https://doi.org/10.1007/BF02084917.

García-Lafuente, J., Cano, N., Vargas, M., Rubín, J.P., Hernández-Guerra, A., 1998. Evolution of the Alboran Sea hydrographic structures during July 1993. Deep Sea Res Part I: Oceanograp. Res. Papers. 45 (1), 39–65. https://doi.org/10.1016/S0967-0637(97)00216-1.

Gaudin, M., Berné, S., Jouanneau, J.M., Palanques, A., Puig, P., Mulder, T., Cirac, P., Rabineau, M., Imbert, P., 2006. Massive sand beds attributed to deposition by dense water cascades in the Bourcart canyon head, Gulf of Lions (northwestern Mediterranean Sea). Mar. Geol. 234 (1–4), 111–128. https://doi.org/10.1016/j.margeo.2006.09.020.

Gerber, T.P., Amblas, D., Wolinsky, M.A., Pratson, L.F., Canals, M., 2009. A model for the long-profile shape of submarine canyons. Case Rep. Med. 114 (3), 1–24. https://doi.org/10.1029/2008JF001190.

Goff, J.A., 2001. Quantitative classification of canyon systems on continental slopes and possible relationship to slope curvature. Geophys. Res. Lett. 28 (23), 4359–4362. https://doi.org/10.1029/2001GL013300.

Gómez de la Peña, L.R., Ranero, C., Gràcia, E., Booth-Rea, G., 2021. The evolution of the westernmost Mediterranean basins. Earth Sci. Rev. 214, 103445 https://doi.org/10.1016/j.earscirev.2020.103445.

Green, A., 2009. Sediment dynamics on the narrow, canyon-incised and current-swept shelf of the northern KwaZulu-Natal continental shelf, South Africa. Geo-Mar. Lett. 29 (4), 201–219. https://doi.org/10.1007/s00367-009-0135-9.

Green, A.N., Goff, J.A., Uken, R., 2007. Geomorphological evidence for upslope canyon forming processes on the northern KwaZulu-Natal shelf, SW Indian Ocean, South Africa. Geo-Mar. Lett. 27 (6), 399–409. https://doi.org/10.1007/s00367-007-0082-2.

Harris, P.T., Macmillan-Lawler, M., 2015. Geomorphology of Mediterranean submarine canyons in a global context – Results from a multivariate analysis of canyon geomorphic statistics. In: Briand, F. (Ed.), Submarine Canyon Dynamics. CIESM, Sorrento, pp. 23–35.

Harris, P.T., Whiteway, T., 2011. Global distribution of large submarine canyons: Geomorphic differences between active and passive continental margins. Mar. Geol. 285 (1–4), 69–86. https://doi.org/10.1016/j.margeo.2011.05.008.

Harris, P.T., Macmillan-Lawler, M., Rupp, J., Baker, E., 2014. Geomorphology of the oceans. Mar. Geol. 352, 4–24. https://doi.org/10.1016/j.margeo.2014.01.011.

Heijnen, M.S., Mienis, F., Gates, A.R., Bett, B.J., Hall, R.A., Hunt, J., Kane, I.A., Pebody, C., Huvenne, V.A.I., Soutter, E.L., Clare, M.A., 2022. Challenging the highstand-dormant paradigm for land-detached submarine canyons. Nat. Commun. 13, 1–11. https://doi.org/10.1038/s41467-022-31114-9.

Hernández-Molina, F.J., Somoza, L., Rey, J., Pomar, L., 1994. Late Pleistocene-Holocene sediments on the Spanish continental shelves: Model for very high resolution sequence stratigraphy. Mar. Geol. 120 (3–4), 129–174. https://doi.org/10.1016/0025-3227(94)90057-4.

Herzer, R.H., Lewis, D.W., 1979. Growth and burial of a submarine canyon off Motunau, North Canterbury, New Zealand. Sediment. Geol. 24 (1–2), 69–83. https://doi.org/10.1016/0037-0738(79)90029-0.

Hill, P.S., Fox, J.M., Crockett, J.S., Curran, K.J., Friedrichs, C.T., Geyer, W.R., Milligan, T. G., Ogston, A.S., Puig, P., Scully, M.E., Traykovski, P.A., Wheatcroft, R.A., 2009. Sediment Delivery to the Seabed on Continental Margins. In: Jarvis, I., Nittrouer, C. A., Austin, J.A., Field, M.E., Kravitz, J.H., Syvitski, J.P.M., Wiberg, P.L. (Eds.), Continental Margin Sedimentation: From Sediment Transport to Sequence Stratigraphy. International Association of Sedimentologists, Special Publication 37. Blackwell Publishing, Oxford, pp. 49–99. https://doi.org/10.1002/9781444304398.ch2.

Hubbard, S.M., Covault, J.A., Fildani, A., Romans, B.W., 2014. Sediment transfer and deposition in slope channels: Deciphering the record of enigmatic deep-sea processes from outcrop. Bull. Geol. Soc. Am. 126 (5–6), 857–871. https://doi.org/10.1130/B30996.1.

Jabaloy-Sánchez, A., Lobo, F.J., Azor, A., Martín-Rosales, W., Pérez-Peña, J.V., Bárcenas, P., Macías, J., Fernández-Salas, L.M., Vázquez-Vílchez, M., 2014. Six thousand years of coastline evolution in the Guadalfeo deltaic system (southern Iberian Peninsula). Geomorphology 206, 374–391. https://doi.org/10.1016/j.geomorph.2013.08.037.

Janocko, M., Nemec, W., Henriksen, S., Warchol, M., 2013. The diversity of deep-water sinuous channel belts and slope valley-fill complexes. Mar. Pet. Geol. 41 (1), 7–34. https://doi.org/10.1016/j.marpetgeo.2012.06.012.

Jimenez-Espejo, F.J., Martinez-Ruiz, F., Rogerson, M., González-Donoso, J.M., Romero, O.E., Linares, D., Sakamoto, T., Gallego-Torres, D., Ruiz, J.L.R., Ortega-Huertas, M., Claros, J.A.P., 2008. Detrital input, productivity fluctuations, and water mass circulation in the westernmost Mediterranean Sea since the Last Glacial Maximum. Geochem. Geophys. Geosyst. 9 (11) https://doi.org/10.1029/2008GC002096.

Jobe, Z.R., Sylvester, Z., Parker, A.O., Howes, N., Slowey, N., Pirmez, C., 2015. Rapid adjustment of submarine channel architecture to changes in sediment supply. J. Sediment. Res. 85 (6), 729–756. https://doi.org/10.2110/jsr.2015.30.

Juan, C., Ercilla, G., Javier Hernández-Molina, F., Estrada, F., Alonso, B., Casas, D., García, M., Farran, M., Llave, E., Palomino, D., Vázquez, J.T., Medialdea, T., Gorini, C., D'Acremont, E., El Moumni, B., Ammar, A., 2016. Seismic evidence of current-controlled sedimentation in the Alboran Sea during the Pliocene and Quaternary: Palaeoceanographic implications. Mar. Geol. 378, 292–311. https://doi.org/10.1016/j.margeo.2016.01.006.

Kane, I.A., McCaffrey, W.D., Peakall, J., 2008. Controls on sinuosity evolution within submarine channels. Geology 36 (4), 287–290. https://doi.org/10.1130/G24588A.1.

Kertznus, V., Kneller, B., 2009. Clinoform quantification for assessing the effects of external forcing on continental margin development. Basin Res. 21 (5), 738–758. https://doi.org/10.1111/j.1365-2117.2009.00411.x.

Lario, J., Zazo, C., Goy, J.L., 1999. Fases de progradación y evolución morfosedimentaria de la flecha litoral de Calahonda (Granada) durante el Holoceno. Estud. Geol. 55, 247–250. https://doi.org/10.3989/egeol.99555-6164.

Lastras, G., Canals, M., Urgeles, R., Amblas, D., Ivanov, M., Droz, L., Dennielou, B., Fabrés, J., Schoolmeester, T., Akhmetzhanov, A., Orange, D., García-García, A., 2007. A walk down the Cap de Creus canyon, Northwestern Mediterranean Sea: recent processes inferred from morphology and sediment bedforms. Mar. Geol. 246 (2–4), 176–192. https://doi.org/10.1016/j.margeo.2007.09.002.

Lastras, G., Arzola, R.G., Masson, D.G., Wynn, R.B., Huvenne, V.A.I., Hühnerbach, V., Canals, M., 2009. Geomorphology and sedimentary features in the Central Portuguese submarine canyons. Western Iberian margin. Geomorphology 103 (3), 310–329. https://doi.org/10.1016/j.geomorph.2008.06.01.

Lastras, G., Canals, M., Amblas, D., Lavoie, C., Church, I., De Mol, B., Duran, R., Calafat, A.M., Hughes-Clarke, J.E., Smith, C.J., Heussner, S., 2011. Understanding sediment dynamics of two large submarine valleys from seafloor data: Blanes and La Fonera canyons, northwestern Mediterranean Sea. Mar. Geol. 280, 20–39. https://doi.org/10.1016/j.margeo.2010.11.005.

Lewis, K.B., Barnes, P.M., 1999. Kaikoura Canyon, New Zealand: active conduit from near-shore sediment zones to trench-axis channel. Mar. Geol. 162 (1), 39–69. https://doi.org/10.1016/S0025-3227(99)00075-4.

Li, J., Li, W., Alves, T.M., Rebesco, M., Wang, X., Li, S., Sun, J., Zhan, W., 2023. Controls on the morphology of closely spaced submarine canyons incising the continental slope of the northern South China Sea. Geomorphology 432, 108712. https://doi.org/10.1016/j.geomorph.2023.108712.

Li, W., Li, S., Alves, T.M., Rebesco, M., Feng, Y., 2021. The role of sediment gravity flows on the morphological development of a large submarine canyon (Taiwan Canyon), north-east South China Sea. Sedimentology 68, 1091–1108. https://doi.org/10.1111/sed.12818.

Liquete, C., Arnau, P., Canals, M., Colas, S., 2005. Mediterranean river systems of Andalusia, southern Spain, and associated deltas: a source to sink approach. Mar. Geol. 222–223 (1–4), 471–495. https://doi.org/10.1016/j.margeo.2005.06.033.

Liu, J.T., Liu, K.J., Huang, J.C., 2002. The effect of a submarine canyon on the river sediment dispersal and inner shelf sediment movements in southern Taiwan. Mar. Geol. 181 (4), 357–386. https://doi.org/10.1016/S0025-3227(01)00219-5.

Lobo, F.J., Fernandez-Salas, L.M., Moreno, I., Sanz, J.L., Maldonado, A., 2006. The sea-floor morphology of a Mediterranean shelf fed by small rivers, northern Alboran Sea margin. Cont. Shelf Res. 26 (20), 2607–2628. https://doi.org/10.1016/j.csr.2006.08.006.

Lobo, F.J., Goff, J.A., Mendes, I., Bárcenas, P., Fernández-Salas, L.M., Martín-Rosales, W., Macías, J., Díaz del Río, V., 2015. Spatial variability of prodeltaic undulations on the Guadalfeo River prodelta: support to the genetic interpretation as hyperpycnal flow deposits. Mar. Geophys. Res. 36 (4), 309–333. https://doi.org/10.1007/s11001-014-9233-9.

Maillard, A., Gorini, C., Mauffret, A., Sage, F., Lofi, J., Gaullier, V., 2006. Offshore evidence of polyphase erosion in the Valencia Basin (Northwestern Mediterranean): scenario for the Messinian Salinity Crisis. Sediment. Geol. 188–189, 69–91. https://doi.org/10.1016/j.sedgeo.2006.02.006.

Marchès, E., Mulder, T., Cremer, M., Bonnel, C., Hanquiez, V., Gonthier, E., Lecroart, P., 2007. Contourite drift construction influenced by capture of Mediterranean Outflow Water deep-sea current by the Portimão submarine canyon (Gulf of Cadiz, South Portugal). Mar. Geol. 242 (4), 247–260. https://doi.org/10.1016/j.margeo.2007.03.013.

Martín, J., Puig, P., Palanques, A., Masqué, P., García-Orellana, J., 2008. Effect of commercial trawling on the deep sedimentation in a Mediterranean submarine canyon. Mar. Geol. 252 (3–4), 150–155. https://doi.org/10.1016/j.margeo.2008.03.012.

Mascle, J., Migeon, S., Coste, M., Hassoun, V., Rouillard, P., 2015. "Rocky" versus "Sedimentary" canyons around the Mediterranean and the Black seas. In: Briand, F. (Ed.), Submarine Canyon Dynamics in the Mediterranean and Tributary Seas. CIESM, Monaco, pp. 37–48.

Mayall, M., Jones, E., Casey, M., 2006. Turbidite channel reservoirs-Key elements in facies prediction and effective development. Mar. Pet. Geol. 23 (8), 821–841. https://doi.org/10.1016/j.marpetgeo.2006.08.001.

Micallef, A., Ribó, M., Canals, M., Puig, P., Lastras, G., Tubau, X., 2014. Space-for-time substitution and the evolution of a submarine canyon-channel system in a passive progradational margin. Geomorphology 221, 34–50. https://doi.org/10.1016/j.geomorph.2014.06.008.

Millot, C., 2009. Another description of the Mediterranean Sea outflow. Prog. Oceanogr. 82 (2), 101–124. https://doi.org/10.1016/j.pocean.2009.04.016.

Millot, C., 2014. Heterogeneities of in-and out-flows in the Mediterranean Sea. Prog. Oceanogr. 120, 254–278. https://doi.org/10.1016/j.pocean.2013.09.007.

Ministerio de Pesca, Agricultura y Alimentación, 2002. Multibeam Bathymetric Grid. Ministerio de Pesca, Agricultura y Alimentación, Spanish Government.

Miralles, J., Radakovitch, O., Aloisi, J.C., 2005. ^{210}Pb sedimentation rates from the Northwestern Mediterranean margin. Mar. Geol. 216 (3), 155–167. https://doi.org/10.1016/j.margeo.2005.02.020.

Mitchell, N.C., 2005. Interpreting long-profiles of canyons in the USA Atlantic continental slope. Mar. Geol. 214 (1–3), 75–99. https://doi.org/10.1016/j.margeo.2004.09.005.

Mitchum Jr., R.M., 1985. Seismic stratigraphic expression of submarine fan. In: Berg, O. R., Woolverton, D.G. (Eds.), Seismic Stratigraphy II: An Integrated Approach to Hydrocarbon Exploration: American Association of Petroleum Geologists, Memoir, vol. 39, pp. 117–136. https://doi.org/10.1306/M39449C7.

Mullenbach, B.L., Nittrouer, C.A., 2000. Rapid deposition of fluvial sediment in the El Canyon, northern California. Cont. Shelf Res. 20 (16), 2191–2212. https://doi.org/10.1016/S0278-4343(00)00067-4.

Mullenbach, B.L., Nittrouer, C.A., Puig, P., Orange, D.L., 2004. Sediment deposition in a modern submarine canyon: Eel Canyon, northern California. Mar. Geol. 211 (1–2), 101–119. https://doi.org/10.1016/j.margeo.2004.07.003.

Muñoz, A., Elvira, E., León, C., Acosta, J., Jiménez, P., 2017. Examples of Sediment Waves in and around Submarine Canyons of the North Alboran Sea. In: Guillén, J., Acosta, J., Chiocci, F.L., Palanques, A. (Eds.), Atlas of Bedforms in the Western Mediterranean. Springer International Publishing, Cham, pp. 247–252. https://doi.org/10.1007/978-3-319-33940-5.

Murray, J.W., 1991. Ecology and Palaeoecology of Benthic Foraminifera. Longman Scientific & Technical, London. https://doi.org/10.4324/9781315846101.

Murray, J.W., 2006. Ecology and applications of Benthic Foraminifera. Cambridge University Press, Cambridge. https://doi.org/10.1017/CBO9780511535529.

Normandeau, A., Lajeunesse, P., St-Onge, G., 2015. Submarine canyons and channels in the lower St. Lawrence Estuary (Eastern Canada): Morphology, classification and recent sediment dynamics. Geomorphology 241, 1–18. https://doi.org/10.1016/j.geomorph.2015.03.023.

Normark, W.R., Carlson, P.R., 2003. Giant submarine canyons: Is size any clue to their importance in the rock record? In: Chan, M.A., Archer, A.W. (Eds.), Extreme Depositional Environments: Mega End Members in Geologic Time: Geological Society of America Special Paper, Boulder, Colorado, vol. 370, pp. 170–190. https://doi.org/10.1130/0-8137-2370-1.175.

Oguz, T., Mourre, B., Tintoré, J., 2017. Modulation of frontogenetic plankton production along a meandering jet by zonal wind forcing: an application to the Alboran Sea. J. Geophys. Res. Ocean. 122 (8), 6594–6610. https://doi.org/10.1002/2017JC012866.

Oliveira, A., Santos, A.I., Rodrigues, A., Vitorino, J., 2007. Sedimentary particle distribution and dynamics on the Nazaré canyon system and adjacent shelf (Portugal). Mar. Geol. 246 (2–4), 105–122. https://doi.org/10.1016/j.margeo.2007.04.017.

Ortega-Sánchez, M., Lobo, F.J., López-Ruiz, A., Losada, M.A., Fernández-Salas, L.M., 2014. The influence of shelf-indenting canyons and infralittoral prograding wedges on coastal morphology: the Carchuna system in Southern Spain. Mar. Geol. 347, 107–122. https://doi.org/10.1016/j.margeo.2013.11.006.

Palanques, A., El Khatab, M., Puig, P., Masqué, P., Sánchez-Cabeza, J.A., Isla, E., 2005. Downward particle fluxes in the Guadiaro submarine canyon depositional system (north-western Alboran Sea), a river flood dominated system. Mar. Geol. 220 (1–4), 23–40. https://doi.org/10.1016/j.margeo.2005.07.004.

Palanques, A., Puig, P., Durrieu de Madron, X., Sanchez-Vidal, A., Pasqual, C., Martín, J., Calafat, A., Heussner, S., Canals, M., 2012. Sediment transport to the deep canyons and open-slope of the western Gulf of Lions during the 2006 intense cascading and open-sea convection period. Prog. Oceanogr. 106, 1–15. https://doi.org/10.1016/j.pocean.2012.05.002.

Parrilla, G., Kinder, T., 1987. Oceanografia física del Mar de Alborán. Bol. Inst. Esp. Oceanogr. 4 (1), 133–165.

Paull, C.K., Caress, D.W., Lundsten, E., Gwiazda, R., Anderson, K., McGann, M., Conrad, J., Edwards, B., Sumner, E.J., 2013. Anatomy of the La Jolla Submarine Canyon system; offshore southern California. Mar. Geol. 335, 16–34. https://doi.org/10.1016/j.margeo.2012.10.003.

Pérez-Asensio, J.N., Aguirre, J., 2010. Benthic foraminiferal assemblages in temperate coral-bearing deposits from the late Pliocene. J. Foramin. Res. 40, 61–78. https://doi.org/10.2113/gsjfr.40.1.61.

Pérez-Belzuz, F., 1999. Geología del Margen y Cuenca del Mar de Alborán durante el Plio-Cuaternario: Sedimentación y Tectónica. Ph.D. Thesis Doctoral,. University of Barcelona, Barcelona, Spain.

Pérez-Belzuz, F., Alonso, B., 2000. Evolución sedimentaria reciente de dos sistemas turbidíticos del área de Motril (NE Alborán). Parte II: Sistema Turbidítico de Sacratif. Geotemas 1 (4), 207–211.

Pérez-Belzuz, F., Alonso, B., Ercilla, G., 2000. Modelos de sistemas turbidíticos en el Área de Motril (NE Alborán). Geotemas 1 (4), 213–216.

Perkins, H., Kinder, T., La Violette, P., 1990. The Atlantic inflow in the Western Alboran Sea. J. Phys. Oceanogr. 20, 242–263. https://doi.org/10.1175/1520-0485(1990)020.

Piper, D.J.W., Normark, W.R., 2009. Processes that initiate turbidity currents and their influence on turbidites: a marine geology perspective. J. Sediment. Res. 79 (6), 347–362. https://doi.org/10.2110/jsr.2009.046.

Platt, J.P., Vissers, R.L.M., 1986. Extensional collapse of thickened continental lithosphere: a working hypothesis for the Alboran Sea and Gibraltar Arc. Geology 17 (6), 540–543. https://doi.org/10.1130/0091-7613(1989)017%3C0540:ECOTCL%3E2.3.CO;2.

Platt, J.P., Whitehouse, M.J., Kelley, S.P., Carter, A., Hollick, L., 2003. Simultaneous extensional exhumation across the Alboran Basin: Implications for the causes of late orogenic extension. Geology 31 (3), 251–254. https://doi.org/10.1130/0091-7613(2003)031<0251:SEEATA>2.0.CO;2.

Popescu, I., Lericolais, G., Panin, N., Normand, A., Dinu, C., Le Drezen, E., 2004. The Danube submarine canyon (Black Sea): Morphology and sedimentary processes. Mar. Geol. 206 (1–4), 249–265. https://doi.org/10.1016/j.margeo.2004.03.003.

Posamentier, H.W., Vail, P.R., 1988. Eustatic controls on clastic deposition II: Sequence and systems tract models. In: Wilgus, C.K., Hastings, B.S., Posamentier, H., Van Wagoner, J., Ross, C.A., Kendall, C.G.St.C. (Eds.), Sea Level Changes: An Integrated Approach: SEPM, Special Publication, vol. 42, pp. 125–154. https://doi.org/10.2110/pec.88.01.0125.

Pratson, L.F., Coakley, B.J., 1996. A model for the headward erosion of submarine canyons induced by downslope-eroding sediment flows. Bull. Geol. Soc. Am. 108 (2), 225–234. https://doi.org/10.1130/0016-7606.

Prins, M.A., Postma, G., Cleveringa, J., Cramp, A., Kenyon, N.H., 2000. Controls on terrigenous sediment supply to the Arabian Sea during the late quaternary: the Indus fan. Mar. Geol. 169 (3–4), 327–349. https://doi.org/10.1016/S0025-3227(00)00086-4.

Puga-Bernabéu, Á., Webster, J.M., Beaman, R.J., Guilbaud, V., 2011. Morphology and controls on the evolution of a mixed carbonate-siliciclastic submarine canyon system, Great Barrier Reef margin, North-Eastern Australia. Mar. Geol. 289 (1–4), 100–116. https://doi.org/10.1016/j.margeo.2011.09.013.

Puga-Bernabéu, Á., Webster, J.M., Beaman, R.J., Guilbaud, V., 2013. Variation in canyon morphology on the Great Barrier Reef margin, North-Eastern Australia: the influence of slope and barrier reefs. Geomorphology 191, 35–50. https://doi.org/10.1016/j.geomorph.2013.03.001.

Puig, P., Palanques, A., Guillén, J., El Khatab, M., 2004. Role of internal waves in the generation of nepheloid layers on the northwestern Alboran slope: Implications for continental margin shaping. J. Geophys. Res. 109 (9), C09011 https://doi.org/10.1029/2004JC002394.

Puig, P., Palanques, A., Orange, D.L., Lastras, G., Canals, M., 2008. Dense shelf water cascades and sedimentary furrow formation in the Cap de Creus Canyon, northwestern Mediterranean Sea. Cont. Shelf Res. 28 (15), 2017–2030. https://doi.org/10.1016/j.csr.2008.05.002.

Puig, P., Palanques, A., Martín, J., 2014. Contemporary sediment-transport processes in submarine canyons. Annu. Rev. Mar. Sci. 6, 53–77. https://doi.org/10.1146/annurev-marine-010213-135037.

Puig, P., Durán, R., Muñoz, A., Elvira, E., Guillén, J., 2017. Submarine canyon-head morphologies and inferred sediment transport processes in the Alías-Almanzora canyon system (SW Mediterranean): on the role of the sediment supply. Mar. Geol. 393, 21–34. https://doi.org/10.1016/j.margeo.2017.02.009.

Rebesco, M., Neagu, R.C., Cuppari, A., Muto, F., Accettella, D., Dominici, R., Cova, A., Romano, C., Caburlotto, A., 2009. Morphobathymetric analysis and evidence of submarine mass movements in the western Gulf of Taranto (Calabria margin, Ionian Sea). Int. J. Earth Sci. 98, 791–805. https://doi.org/10.1007/s00531-009-0429-1.

Renault, L., Oguz, T., Pascual, A., Vizoso, G., Tintore, J., 2012. Surface circulation in the Alborn Sea (western Mediterranean) inferred from remotely sensed data. J. Geophys. Res. Ocean. 117 (8), 1–11. https://doi.org/10.1029/2011JC007659.

Rodriguez, M., Maleuvre, C., Jollivet-Castelot, M., d'Acremont, E., Rabaute, A., Lafosse, M., Ercilla, G., Vázquez, J.T., Alonso, B., Ammar, A., Gorini, C., 2017. Tsunamigenic submarine landslides along the Xauen-Tofiño banks in the Alboran Sea (Western Mediterranean Sea). Geophys. J. Int. 209 (1), 266–281. https://doi.org/10.1093/gji/ggx028.

Ryan, W.B.F., Hsu, K.J., Cita, M.B., Dumitricia, P., Lort, J., Maync, W., Nesteroff, W.D., Pautot, G., Stradner, H., Wezel, F.C., 1973. Western Alboran Basin — Site 121. Initial reports of the Deep Sea Drilling Project 13. U.S. Govt. Printing Office, Washington D. C., p. 1447

Sarhan, T., Lafuente, J.G., Vargas, M., Vargas, J.M., Plaza, F., 2000. Upwelling mechanisms in the northwestern Alborán Sea. J. Mar. Syst. 23 (4), 317–331. https://doi.org/10.1016/S0924-7963(99)00068-8.

Schmiedl, G., de Bovée, F., Buscail, R., Charrière, B., Hemleben, C., Medernach, L., Picon, P., 2000. Trophic control of benthic foraminiferal abundance and microhabitat in the bathyal Gulf of Lions, western Mediterranean Sea. Mar. Micropaleontol. 40, 167–188. https://doi.org/10.1016/S0377-8398(00)00038-4.

Serrano, M.A., Díez-Minguito, M., Valle-Levinson, A., Ortega-Sanchez, M., 2020. Circulation in a short, Microtidal Submarine Canyon in the Alborán Sea. J. Coast. Res. 95 (1), 1531–1535. https://doi.org/10.2112/SI95-295.1.

Shepard, F.P., 1981. Submarine canyons: multiple causes and long-time persistence. Am. Assoc. Petr. Geol. B. 65 (6), 1062–1077. https://doi.org/10.1306/03B59459-16D1-11D7-8645000102C1865D.

Shepard, F.P., Emery, K.O., 1941. Submarine Topography off the California Coast: Canyons and Tectonic Interpretation. Geol. Soc. Am. Spec. Pap. 31, 171. https://doi.org/10.1130/SPE31.

Smith, M.E., Werner, S.H., Buscombe, D., Finnegan, N.J., Sumner, E.J., Mueller, E.R., 2018. Seeking the Shore: evidence for active submarine canyon head incision due to coarse sediment supply and focusing of wave energy. Geophys. Res. Lett. 45 (22), 12,403–12,413. https://doi.org/10.1029/2018GL080396.

Soutter, E.L., Kane, I.A., Hodgson, D.M., Flint, S., 2021. The concavity of submarine canyon longitudinal profiles. J. Geophys. Res. 126 (10), e2021JF006185 https://doi.org/10.1029/2021JF006185.

Stanley, D.J., Kelling, G., Juan-Antonio Vera, J.-A.V., Sheng, H., 1975. Sands in the Alboran Sea: A Model of Input in a Deep Marine Basin. Smithson. Contrib. Earth Sci. 15, 1–51. https://doi.org/10.5479/si.00810274.15.1.

Sweet, M.L., Blum, M.D., 2016. Connections between fluvial to shallow marine environments and submarine canyons: Implications for sediment transfer to deep water. J. Sediment. Res. 86 (10), 1147–1162. https://doi.org/10.2110/jsr.2016.64.

Tintoré, J., La Violette, P.E., Blade, I., Cruzado, A., 1988. A Study of an intense Density Front in the Eastern Alboran Sea: the Almeria Oran Front. J. Phys. Oceanogr. 18 (10), 1384–1397. https://doi.org/10.1175/1520-0485(1988)018%3C1384:ASOAID%3E2.0.CO;2.

Tubau, X., Lastras, G., Canals, M., Micallef, A., Amblas, D., 2013. Significance of the fine drainage pattern for submarine canyon evolution: the Foix Canyon System, Northwestern Mediterranean Sea. Geomorphology 184, 20–37. https://doi.org/10.1016/j.geomorph.2012.11.007.

Tubau, X., Canals, M., Lastras, G., Rayo, X., Rivera, J., Amblas, D., 2015. Marine litter on the floor of deep submarine canyons of the Northwestern Mediterranean Sea: the role of hydrodynamic processes. Prog. Oceanogr. 134, 379–403. https://doi.org/10.1016/j.pocean.2015.03.013.

Udden, J.A., 1914. Mechanical composition of clastic sediments. Bull. Geol. Soc. Am. 25 (1), 655–744. https://doi.org/10.1130/GSAB-25-655.

Vail, P.R., 1987. Part 1: Seismic stratigraphy interpretation procedure. In: Bally, A.W. (Ed.), Atlas of Seismic Stratigraphy, Volume 1, Am. Assoc. Petr. Geol. B, vol. 27, pp. 1–10.

Vázquez, J.T., Ercilla, G., Alonso, B., Juan, C., Rueda, J.L., Palomino, D., Fernández-Salas, L.M., Bárcenas, P., Casas, D., Díaz-del-Río, V., Estrada, F., Farran, M., García, M., González, E., López-González, N., El Moumni, B., Contouriber, M.A.M.T., 2015. Submarine canyons and related features in the Alboran Sea: Continental margins and major isolated reliefs. In: Briand, F. (Ed.), Submarine Canyon Dynamics in the Mediterranean and Tributary Seas. CIESM, Monaco, pp. 183–196.

Walsh, J.P., Nittrouer, C.A., 2003. Contrasting styles of off-shelf sediment accumulation in New Guinea. Mar. Geol. 196 (3–4), 105–125. https://doi.org/10.1016/S0025-3227(03)00069-0.

Warrick, J.A., 2014. Eel River margin source-to-sink sediment budgets: Revisited. Mar. Geol. 351, 25–37. https://doi.org/10.1016/j.margeo.2014.03.008.

Weaver, P.P.E., Pujol, C., 1988. History of the last deglaciation in the Alboran Sea (western Mediterranean) and adjacent North Atlantic as revealed by coccolith floras. Palaeogeogr. Palaeoclimatol. Palaeoecol. 64 (1–2), 35–42. https://doi.org/10.1016/0031-0182(88)90140-X.

Wentworth, C.K., 1922. A scale of grade and class terms for clastic sediments. J. Geol. 30 (5), 377–392.

Wiles, E., Green, A., Watkeys, M., Botes, R., Jokat, W., 2019. Submarine canyons of NW Madagascar: A first geomorphological insight. Deep. Res. Part II Top. Stud. Oceanogr. 161, 5–15. https://doi.org/10.1016/j.dsr2.2018.06.003.

Xu, J.P., Wong, F.L., Kvitek, R., Smith, D.P., Paull, C.K., 2008. Sandwave migration in Monterey Submarine Canyon, Central California. Mar. Geol. 248 (3–4), 193–212. https://doi.org/10.1016/j.margeo.2007.11.005.

Zúñiga, D., Flexas, M.M., Sanchez-Vidal, A., Coenjaerts, J., Calafat, A., Jordà, G., García-Orellana, J., Puigdefàbregas, J., Canals, M., Espino, M., Sardà, F., Company, J.B., 2009. Particle fluxes dynamics in Blanes submarine canyon (Northwestern Mediterranean). Prog. Oceanogr. 82 (4), 239–251. https://doi.org/10.1016/j.pocean.2009.07.002.